PFC/RR-88-11 DOE/ET-51013-254

The Physics and Engineering of Alcator C-MOD

I. H. Hutchinson, H. Becker, P. Bonoli, N. Diatchenko,
S. Fairfax, C .Fiore, R. Granetz, M. Greenwald, D. Gwinn,
S. Hakkarainen, D. Humphreys, J. Irby, B. Lipschultz,
E. Marmar, D. B. Montgomery, C. Park, R. Parker, N. Pierce,
R. Pillsbury, M. Porkolab, J. Ramos, J. Rice, J. Schultz,
D. Sigmar, F. Silva, Y. Takase, J. Terry, E. Thibeault, S. Wolfe
Plasma Fusion Center
Massachusetts Institute of Technology
Cambridge, MA 02139

August 1988

This work was supported by the U. S. Department of Energy Contract No. DE-AC02-78ET51013. Reproduction, translation, publication, use and disposal, in whole or in part by or for the United States government is permitted.

THE PHYSICS AND ENGINEERING OF ALCATOR C-MOD

I.H.Hutchinson, H.Becker, P.Bonoli, N.Diatchenko, S.Fairfax, C.Fiore, S.Golovato, R.Granetz, M.Greenwald, D.Gwinn, S.Hakkarainen, D.Humphreys, J.Irby, B.Lipschultz, E.Marmar, D.B.Montgomery, C.Park, R.Parker, N.Pierce, R.Pillsbury, M.Porkolab, J.Ramos, J.Rice, J.Schultz, D.Sigmar, F.Silva, Y.Takase, J.Terry, E.Thibeault, S.Wolfe

Plasma Fusion Center,
Massachusetts Institute of Technology,
Cambridge, Massacusetts, U.S.A.

Abstract

Alcator C-Mod is a new tokamak under construction at M.I.T. that promises to play an important and flexible role in the international fusion research effort. The physics and engineering features of the tokamak are described, giving an overview of the machine and plasma configurations. On the basis of empirical scaling laws, we predict the plasma confinement performance to be near DT equivalent breakeven. The planned experimental program is addressed to many of the vital physics questions still uncertain in high-performance tokamak plasma behaviour as well as to the investigation of innovative approaches to tokamak improvement.

1 Background

The high-field compact tokamak approach to plasma confinement has proven to be extremely successful in obtaining hot, well confined plasmas in machines of modest size and cost. Pioneered by Alcator A in the 1970s, and extended by Alcator C and FT, this type of high-performance tokamak is firmly established as an attractive device for pursuing plasma and fusion research into the ignited regime. In many respects the proposed compact ignition tokamak (CIT) experiment follows in this tradition.

Alcator C achieved[1] a value of the product of density (n_e) and energy confinement time (τ_E) of about 8×10^{19} $m^{-3}s$. It was thus the first magnetic confinement device to exceed the minimum value of the Lawson parameter required for energy breakeven. Despite the many much larger tokamaks that are now in operation, this achievement has been exceeded by only one experiment to date[2].

In the development of basic plasma understanding and of the ability to predict tokamak behaviour, the Alcator devices have also been extremely productive. Examples of discoveries that now influence the wider fusion effort include the ohmic confinement "Alcator" and "NeoAlcator" scalings[3], the influence of density-profile peaking on improving confinement[4] (p-mode), the demonstration of noninductive current drive at high density[5], as well as numerous other significant advances in knowledge and technique.

Despite its successful and productive past performance, Alcator C, like Alcator A, was traditional in its design. It had a circular cross-section plasma, its edge was defined by a solid limiter, and the level of auxilliary heating was modest, less than the normal ohmic heating power. In addition, because of their monolithic Bitter-plate construction, Alcator A and C had very limited port access. The small ports imposed severe constraints on the flexibility and quantity of auxiliary heating, as well as the diagnostic experiments. For these reasons, and because the configuration under consideration for CIT demanded the exploration of other important issues, the new experiment Alcator C-Mod was proposed.

Alcator C-Mod arose conceptually as a modification of the older machine, Alcator C. However, it soon became clear that the most effective way to achieve the aims of the experiment was to build an assembly that was almost

entirely new, while utilizing the extensive ancillary equipment (prime power, convertors, diagnostics, etc.) available from the Alcator C program. Alcator C-Mod incorporates such modern tokamak design features as: shaped non-circular plasma cross-section, a poloidal divertor configuration, and dominant (ICRF) auxilliary heating. In addition the port access is greatly increased, allowing direct personnel access to the interior of the vacuum vessel and hence much greater flexibility in the internal hardware.

The Alcator C-Mod proposal[6] (Oct 1985) provided detailed information on the rationale, physics and engineering of the original experimental design; a subsequent addendum[7] (Apr 1986) describes the changes to that design that were made to reduce its costs, in the face of U.S. fusion budget cuts. Since a year elapsed before final approval for the construction was received (Apr 1987), further evolution of the plans and refinement of the engineering are now being incorporated into the experiment. It is the purpose of this report to describe the machine that is now being built.

2 Objectives

Alcator C-Mod will serve in two main roles: first as a vehicle for extending the plasma regimes and experimental capability of high-performance tokamaks, enabling the exploration of new physics and engineering concepts and the investigation of plasma performance in fusion plasmas; second as a prototype for the CIT, of which Alcator C-Mod is in many respects a scaled version. These two roles are complementary. The physics research program of Alcator C-Mod is valuable in its own right, representing as it does the next logical step in high-performance tokamak research. This program fits well with the desire to support experimentally the design and physics of CIT, which strongly influences C-Mod's configuration and experimental plan.

The specific objectives of the Alcator C-Mod project may be summarized as follows:

Explore and assess the confinement performance of an ohmically heated compact high-field tokamak with advanced shaping.

Evaluate ICRF performance at high density in a shaped, diverted high-field tokamak and establish its applicability to ignition conditions.

Study and optimize the operation of different divertor configurations at high density, especially their influence on confinement, with multi-megawatt auxilliary heating.

Investigate the viability of control of the profiles of density (via pellets), temperature and current profile (via RF), together with plasma shaping and edge and impurity control (divertor) for enhanced stability and confinement.

Ohmic ignition in a tokamak is an objective that has received renewed interest recently[8], in part because of the observed degradation of confinement with auxilliary heating power. However, major uncertainties exist in the anticipated confinement at the high densities and currents necessary, as well as in the extent of improvement possible through plasma shaping. Alcator C-Mod can contribute to the knowledge and understanding necessary to judge the feasibility of ohmic ignition.

Heating in the Ion Cyclotron Range of Frequencies (ICRF) is currently the planned heating scheme for CIT. It has many potential advantages over Neutral Beam Injection heating; however there is very little experience of its operation in high-density tokamaks. Alcator C-Mod offers the opportunity of testing both the physics and the engineering of ICRF heating in the parameter regimes relevant to compact ignition devices.

In recent years it has become clear[9] that edge plasma conditions can have a strong influence on the bulk confinement performance of tokamaks. Also, the power densities required in compact fusion devices set a high priority on obtaining control of the plasma-wall interactions so as to minimize their deleterious effects. Alcator C-Mod will be the first tokamak capable of operation with electron densities substantially above 10^{20} m^{-3} in a divertor configuration. It will thus provide information of great importance to future ignition devices.

An ongoing theme for future tokamak development is likely to be control. Alcator C-Mod will be able to extend the investigation of density profile control with pellets and pursue the optimization of other shape and profile parameters as well as developing practical techniques for their control.

3 Alcator C-Mod Design Parameters.

The basic plasma design parameters of Alcator C-Mod are shown in Table 1.

Table 1. Alcator C-Mod Parameters.

Major Radius	R	=	0.665 m.
Minor Radius	a	=	0.21 m.
Toroidal Field	B_T	=	9 T.
Plasma Current	I_p	=	3 MA.
Elongation	κ	=	1.8 (typical).
Triangularity	δ	=	0.4 (typical).
Flat-top Duration			1 s (@ 9T)
			7 s (@ 5T)
Inductive Volt-seconds			7.5 Wb.
Required energy			500 MJ.

These parameters constitute perhaps the highest performance machine consistent with the available pulsed energy from Alcator's alternator. They are made possible together with the improved port access by the design concepts illustrated in the overall machine drawings Figs. 1 and 2.

The toroidal field (TF) magnet is constructed from twenty discrete rectangular coils, each having six turns, which have sliding joints at each corner. The magnetic loads on these coils are taken by a massive stainless steel support structure surrounding the magnet assembly. The poloidal field coils (except for one pair) are inside the TF. They are responsible for the combined tasks of providing inductive current-drive, plasma equilibrium and plasma shaping. They are mounted on the stainless steel vacuum vessel, which is thus a structural element as well as the primary vacuum chamber. All the magnets are copper, cooled to liquid nitrogen temperature prior to a plasma shot. A cryogenic dewar surrounds the whole machine.

4 Toroidal Field Engineering

4.1 Sliding Joints

The sliding joints for the TF magnets have proven to be an ambitious engineering development program for Alcator C-Mod. These joints must be capable of high current densities, while undergoing substantial deflections under coil in-plane and out-of-plane loads. The overall joint and TF magnet assembly concepts are shown in Fig. 3. The current-joint specifications and loads are shown in Table 2.

Table 2. Sliding Joint Specifications.

Number of joints	480
Current per turn	0.25 MA
Average face current density	20 MA m^{-2}
Peak face current density	43 MA m^{-2}
Maximum allowed surface resistance	1 nΩ m^2
Relative vertical sliding movement	$\pm$1 mm
Relative radial sliding movement	0.5 mm
Number of cycles	50000.

Early tests on sliding joint concepts identified surface preparations with excellent resistivity and wear properties. However, the addition of coatings to broad copper fingers failed in full-scale joint tests because of the inability to achieve uniform contact over a broad area in a practical assembly. Multilams have been used with other jointed designs to provide multiple contacts over a broad area, but because of the long length of the lams, they have an intrinsically high resistance. Various multilam materials and shapes were tested. The current density was extended considerably over previous benchmarks, but the concept was marginal for C-MOD.

Feltmetal pads were identified as a new concept that combined the best features of flat plates and multilams. There are numerous contacts at the felt pad surfaces, but the underlying matrix is tough and has high conductivity.

Separate spring plates provide a preload pressure between the faces of 2.75 MPa, while allowing normal displacements up to 0.3mm without losing electrical contact. The joints are also designed to allow the calculated relative sliding movements of 1 mm verically and 0.5 mm radially. Extensive testing of feltmetal sliding joints have shown them to be well able to meet the specifications for performance and durability, provided that sufficient face pressure is maintained. An analysis of stresses, displacements, current and temperature distribution in the finger region led to shaping of the fingers and feltmetal pads, as shown in Fig. 4. The fingers have been tapered to allow the contacts to follow out-of-plane displacements instead of rocking about the edge of the contact area. The feltmetal contacts were reduced to four pads, instead of covering the entire available contact surface, in order to ensure good contact in the leading edge region where the joint current is concentrated.

4.2 TF Central Column.

The inside legs of the 120 turns in the TF magnet are wedge-shaped vertical plates, bonded into a monolithic central colum. This assembly supports the radial centering loads on the TF magnets through wedging, and supports a fraction of the vertical loads through tension.

Without reinforcement, the combined loads on the plates would cause a stress intensity at the inner bore region exceeding copper yield strength. Steel plates between the wedge-shaped copper half-conductors prevent the copper from yielding. The reinforcement plates are extended on the inside to serve double duty as cooling fins. The wedged conductors are C-10700 copper, bonded to flat 216 stainless-steel plates, with an average 4:1 copper/reinforcement ratio over the central column area. The yield strength of the copper is 310 MPa, up to 100 ^{0}C, while the yield strength of the steel plates is 1200 MPa. The peak Tresca stress on the steel at the inside radius is calculated to be 580 MPa, while that in the copper is 310 MPa. This type of laminated structure was found to perform very well on Alcator C.

4.3 External Superstructure

Because of the sliding joints, the forces on the TF magnets, other than

those on the central column, must be supported by an external stainless steel superstructure. Vertical forces on the TF horizontal legs are supported by the top and bottom domes. Out-of-plane loads are transmitted to wedge plates, between the horizontal legs of the TF coils. The domes and wedge plates are both bolted to an outer structural cylinder that supports vertical and out-of-plane loads through the bolted connections, and also directly supports the outward radial loads on the outer vertical legs of the TF magnet. These structures are illustrated in Figs. 1 and 2.

Each of the two domes is machined from a single 26 tonne 316 LN forging. The domes are sufficiently thick to support the distributed vertical load from the TF magnet legs in bending without approaching static allowables, so that cyclic loading governs the design. The highest stress in the cover is 370 MPa at the vertical port apertures. The machine will be inspected every 12-15,000 full-field cycles. Assuming initial cracks of 2.5 mm, a safety factor of five against crack growth to 25 mm was calculated.

The stresses in the outer cylinder are generally lower than those in the domes. However, vertical forces are transmitted from the dome to the cylinder through vertical draw bars, pinned horizontally to the cylinder. The highest local stress anywhere in the superstructure is at the pin holes of the drawbars. The draw bars are made of high strength Inconel 718, so that this region is less limiting than the port cutouts in the domes.

5 Poloidal Field Coil System

The poloidal field coil system may be thought of as consisting of the ohmic heating (OH) primary coil and the equilibrium field (EF) coils. Actually the roles of the coils are a mixture of these functions but we refer to the central solenoid as the OH coil and to the others as the EF coils, reflecting their dominant assignments.

The central solenoid consists of three independently controllable coils: OH1, OH2-upper, and OH2-lower. As illustrated in Fig. 5, OH1 is a notched coil which extends the full height of the stack but has the full thickness only in the central one third of the height. It is wound in place on the central core of the TF from continuous solid copper conductor. This necessitates certain cross-over windings between layers which complicate the coil design somewhat. The OH2 sections fill in the remaining volume to make up a complete solenoid

whose current density profile can be varied even though the leads to the separate sections need to connect only to the ends of the solenoid. The whole coil is cooled by liquid nitrogen forced through passages on the inner and outer faces.

The coils EF1-3 are the main coils responsible for plasma equilibrium and shaping. They are supported directly from the thick vacuum vessel (see Fig 2.). A smaller coil, EFC, is used for fast control of the plasma vertical position which otherwise experiences an axisymmetric instability. An additional coil EF4 is mounted outside the cylinder of the superstructure. It gives added flexibility to the plasma shapes and field gradients available. However, because of the slow penetration of the fields through the structure, its current can only be changed relatively slowly, on a timescale ~200 ms.

6 Vacuum Vessel and Wall Hardware

The vacuum vessel is a thick, welded 304L stainless steel structure, as illustrated in Fig.6. It is designed to support all the loads generated by currents in the poloidal field windings and in the vessel itself, under normal operating conditions and during disruptions. The current decay rate assumed for the disruptions is 1MA/ms, which induces very large currents in the vessel. The use of a thick, rather low resistance, vessel is something of a departure from past tokamak practice. Previous machines have minimised the shorting effect of a conducting vessel either by adopting a thin bellows construction, to increase resistance, or by introducing an insulating break in the vessel. In Alcator C-Mod neither of these expedients is adopted since they would preclude the use of the vessel as a key structural element. Instead, the large toroidal vessel current (perhaps as much as 0.4 MA during breakdown) will be tolerated and the perturbing poloidal fields will be compensated by control of the winding currents.

The horizontal access ports are 0.20m wide and 0.63m high, allowing direct personnel access to the interior. The ports prove to be an area to which special engineering attention must be paid. The non-axisymmetric currents which flow in the vessel past the ports induce large magnetic forces there. Also the penetration of the ports through the superstructure cylinder requires demountable connections inside the cylinder for assembly. These large connections have to withstand the thermal cycling (possibly to liquid nitrogen

temperatures), and eddy current forces, without leaks.

The surfaces directly in contact with the plasma edge, the inner bumper limiter and the divertor plates, are protected by tiles. The peak heat load on the tiles due to plasma interaction is estimated to be about 10 MW/m^2, under normal operation, which includes a factor of 2 enhancement due to incomplete toroidal symmetry. However, during disruptions the power density may reach 1000 MW/m^2 which will undoubtedly cause evaporation of whatever material is used. As materials, molybdenum and graphite have been used in comparable situations in previous experiments. They are both able to withstand the normal heat load without damage. Both are under active consideration.

The hardware is designed so that by making the separatrix scrape off into the bottom of the machine a "closed" divertor configuration is obtained, maximizing the trapping of neutral particles in the divertor chamber. However, the top of the machine allows an "open" divertor configuration, so comparison of the performance of different configurations can be made without internal hardware changes. Particularly in the closed configuration, the pumping requirements for the divertor chamber are anticipated to be very large, as high as 10^4 ls^{-1}. Zirconium-Aluminum or similar getter panels are under consideration for this pumping since the conductance of the vertical ports is relatively small, their size being limited by the toroidal field coil and superstructure dome.

During plasma pulses, recycled gas in the vacuum chamber can be expected to raise the pressure as high as perhaps 0.01 mbar near scrape-off hardware. However, to ensure maximum plasma purity, the base pressure of the vacuum system when not operating plasmas is in the UHV range (typically $< 10^{-11}$bar). Internal components are specified for outgassing so that this base pressure can be achieved with the anticipated 1000 l/s pumping speed of the turbomolecular pumps. Baking of the vessel to 150^0C is specified to assist in initial outgassing, and further cleaning of exposed surfaces prior to plasma operation will be performed with glow- and repetitive pulse-discharge cleaning.

7 Control System and Data Acquisition

Control of the various subsystems of the machine will be through a number of elements: transducers, programmable logic controllers (PLCs), CAMAC

equipment, hardwired circuits, and user terminals.

For slow monitoring and control the PLCs provide excellent multipurpose interfaces between the distributed intelligence network and the hardware under control. Approximately 3000 control/monitor points will be serviced by about 15 PLCs. The advantages of such an approach include: cleaner layout and reduced wiring, modularity and redundancy, ease of documentation, maintenance and expansion, and versatile fault handling. The PLCs can communicate directly with one another via a peer link but main high-level communication will be via a networked set of processors, probably IBM PC type.

For sequencing and wave-form generation, CAMAC bus and microVax units will be used. This approach allows much faster programming than the PLCs and draws on experience gained with data acquisition hardware and software in similar configurations.

The real-time feedback control of the plasma, for example its position, current shape and so on, will be accomplished using a hybrid analog/digital system. This will consist of a large (up to 50×10) matrix whose coefficients are programmable digitally. The matrix can be updated ~500 times during the course of the plasma shot, at a minimum update time of approximately 1ms. Inputs from the numerous plasma sensors are multiplied by this matrix to give derived plasma quantities which can then be passed through programmable PID controllers and a further similar matrix multiplication stage to provide demand signals for power supplies etc. The resulting system is extremely fast in its response to plasma changes because the multiplications are analog, capable of responding on the microsecond timescale. It is also very flexible because of the ability to program arbitrarily the control matrices.

Anticipated needs for data acquisition during the operation of the experiment are approximately 10 Mbytes per shot in 1000 channels. This will employ a variety of different acquisition hardware units operated through CAMAC, controlled by a VAX8350 via an optically linked serial highway. Additional cpu power will be available in clustered VAXstations. Data will be stored on a farm of disks using an expanded version of MDS, the model data system developed at MIT. A heirachical data structure will provide ready access to data via the main servers. Much of the user analysis will be done on individual VAXstations. The solutions adopted for the Alcator C-Mod data system are part of a collaborative effort with Los Alamos National Laboratory and the Istituto Gas Ionizzati, Padova (Italy).

8 Power Supplies

The peak power demand of Alcator C-MOD will approach 400 MVA, with roughly 500 MJ delivered energy per pulse. Nearly half of this energy is stored in the toroidal magnetic field of the machine.

The prime power source is a 225 MVA turbine generator built in 1952. After 25 years of service for Consolidated Edison, the unit was retired and donated to MIT. During the period 1978-1987, the alternator supplied over 100,000 power pulses to Alcator C with only 3 days unscheduled outage. The alternator is driven by a 2000 horsepower wound-rotor induction motor and stores 530 MJ at 1800 rpm in the 120-ton rotor.

The higher power and energy requirements of Alcator C-MOD require significant changes in the alternator. A flywheel weighing about 80 tons will be installed to increase the stored energy. An extensive inspection of the rotor and stator will be undertaken. If necessary, cracks in the rotor bore will be machined out and the stator end turns will be braced to assure adequate safety factors for the proposed duty. A comprehensive monitoring and inspection program will be implemented to assure the continued integrity of the alternator.

The toroidal field power supply converter uses a tapped transformer and 2 thyristor bridges to implement a sub-cycle load tap changer and reduce peak power demand to the alternator. At low currents, the bridge connected to the high-voltage tap provides all the DC current. As the AC current flow from the alternator approaches a pre-set limit (roughly equal to the full-load current rating of the alternator) the high-voltage bridge is phased back and the DC load current is commutated to the low-voltage bridge. At full DC current of 250 KA, the high-voltage bridge is entirely off. Since the low-voltage bridge demands only 1/2 the AC line current as the high-voltage bridge, the alternator power demand is greatly reduced. This scheme reduces the stresses in the alternator while forcing the TF magnet current up and down quickly so as to minimize dissipated energy and recool time between pulses.

The poloidal field power converters total over 200 MVA. In order to allow flexible plasma shaping and position control, most coils have separate converters. All but the fast vertical position converter will be conventional

6 or 12-pulse line-commutated units. The vertical position coils require a switchmode converter with a full-power bandwidth of roughly 1 KHz.

9 MHD Configuration

A major advance over the previous Alcator C that C-Mod represents is the ability to study shaped plasma cross-sections. The production of these shapes is, of course, the function of the poloidal field system. Extensive exploration of possible coil configurations, using codes that solve numerically the MHD equilibrium equations of the plasma for specified coil currents and positions, have led to the final coil design. This design represents a trade-off between the desire for flexibility and the necessity to operate at high currents. Flexibility is generally improved by having more coil sets in different locations. High-current performance is generally favoured by having fewer, larger coils and minimizing the extent to which neighbouring coil currents oppose one another. The coil set chosen is judged, on the basis of our code studies, to represent a good compromise.

The equilibrium that we take as standard is illustrated in Fig. 7. It has a current of 3 MA at a toroidal field of 9 T. Qualitatively, the currents in the OH coil determine the flux swing that drives the plasma current. For full-performance cases such as that illustrated, the OH transformer currents are swung from maximum forward to maximum reverse during the course of the plasma shot. The limits are imposed essentially by the magnetic stresses in the coil. At the instant depicted in Fig. 7 there is a significantly larger (negative) current in the OH1 than OH2. This has an important effect on the plasma shape, helping to "push" on the midplane. Together with the "pull" that the positive currents in EF1, and to a lesser extent EF2, exert on the plasma, these currents cause the plasma to become vertically elongated, as shown. EF3 and EF4 contribute somewhat to the shaping but their major role is to provide the vertical field that gives a force in the major radial direction to balance the tendency of the plasma to expand. Coils EF1 and EF3 are, in some configurations, close to stress limits. Also their temperature rise during a pulse can be very significant, as much as 200 ^{o}C.

The profiles of toroidal current density and safety factor, q, for this standard equilibrium are shown in Fig. 8. The equilibrium is deliberately

constrained to have q≈1 on axis. Its value at the 95% flux surface is about 2.3. The current profile is not unduly flat for this beta value (β_p=0.3), the pressure profile has been taken as

$$p \propto \frac{e^{-\alpha}[\ 1 + (1-\bar{\psi})\alpha\ ] - e^{-\alpha\bar{\psi}}}{\alpha(e^{-\alpha} - 1)} ,$$

where $\bar{\psi} = (\psi-\psi_0)/(\psi_e-\psi_0)$ is the normalized poloidal flux, and the profile parameter, α, is equal to -2.37.

The up-down asymmetry in currents deliberately introduced in Fig. 7 gives rise to a single-null divertor configuration, in which the flux surfaces scrape off into the bottom divertor chamber. As well as being able to invert the asymmetry and run upper-divertor plasmas, the plasma can be run with a symmetric double-null divertor, as illustrated in Fig. 9.

We anticipate that the plasma will be initiated as a near-circular cross-section and grown to the final shape as the pulse evolves and the plasma current rises. In Fig. 9 is shown the sequence of shapes obtained during a simulation of the current rise calculated with the combined equilibrium-transport code TSC[10]. The corresponding evolution of the main plasma parameters is shown in Fig. 10. Simulations such as this also take account of the axisymmetric eddy currents in the vacuum vessel and demonstrate the ability of the coil set to provide appropriate control even in the presence of the conducting structures.

An issue of special concern is the provision of an adequate field null at the time of breakdown, together with sufficient toroidal loop voltage to cause ionization and current rise. An electromagnetic model of the entire machine including the superstructure, illustrated in Fig. 11, has been used to demonstrate the feasibility of obtaining an appropriate field null with gradient no more than 0.01 T/m, and favourable evolution, in the presence of a loop voltage of as much as 20 V at the plasma.

The vertical elongation inevitably induces an axisymmetric instability consisting of a vertical motion of the plasma. The conducting structures around the plasma, notably the vacuum vessel, suppress this instability so that it no longer takes place on the Alfven timescale (typically submicro-second). However the finite resistivity of the vessel allows the instability to proceed on the much slower timescale of the resistive decay of the eddy currents in the vessel. In order to stabilize the mode entirely, a feedback-control system must be implemented which senses the plasma position and

applies an appropriate horizontal field to hold its vertical position. Since Alcator C-Mod has substantial elongation, comparable to the maximum demonstrated in past tokamaks, extensive studies have been undertaken to verify the stabilizing scheme. The model used[11] is one in which the plasma is represented by a set of current filaments and the vessel is approximated by a discrete set of conductors. The results show that effective stabilization is possible for elongations up to ~2.1 provided that a rather fast control system and power supply (response time < ~0.5 ms) is used.

10 Radio Frequency Heating

The use of wave heating in the Ion Cyclotron Range of Frequencies is attractive for the high density plasmas needed for fusion ignition because the more widely studied neutral beam heating suffers severe difficulties both in access to the plasma and in penetration to its center. By contrast ICRF has more compact plasma-access requirements, has no known relevant density limitation as such, and can in principle control the location of the power deposition relatively straightforwardly. Its major difficulty is that it does require a launching antenna very close to the edge of the plasma. Moreover, the experimental experience with ICRF, especially at high magnetic fields and densities is rather limited. This, of course, is one reason for the importance of the Alcator C-Mod experiments.

The ICRF heating plans for Alcator C-Mod take advantage of the availability of surplus (FMIT) RF generating units that can be upgraded at moderate cost to provide 2 MW each at a frequency of 80 MHz. MIT is currently funded to upgrade two of these units, although two more are available and should provide a valuable extension in the scope of the program. The waves launched damp on specific species in the plasma close to certain harmonics of the ion cyclotron frequencies. In Fig. 12 are shown the relevant resonances as functions of magnetic field. This graph shows that Alcator C-Mod can undertake fast-wave heating experiments on Helium-3 (He^3) minority species in deuterium (D) plasmas at about 8 T magnetic field, hydrogen (H) minority in deuterium at 5 T, and Ion Bernstein Wave (IBW) heating at 3/2 times the deuteron cyclotron frequency at 7 T. These are the main schemes planned. They require operation with deuterium which adds to the project cost because, at the anticipated temperatures and densities, the neutron emission from DD fusion reactions

demands an experimental cell with substantial shielding. Nevertheless the versatility afforded by deuterium operation and the ability to explore D(He^3) heating, which is analogous to schemes under consideration for CIT, justifies the expense.

The configuration of the proposed fast-wave antenna within Alcator C-Mod is illustrated in Fig. 13. Major concerns for the antenna design include: wave spectrum launched, wave coupling through the edge plasma, avoidance of arcing in antenna or feedlines, and use of a Faraday shield to provide the optimum wave polarization and prevent direct plasma contact to the current strap. Areas of specific interest in the context of compact, high performance tokamaks include the forces induced in the antenna structure at disruptions, the limits on power density that can be launched (up to 2 kW/cm^2 is planned), and impurity generation during fast-wave heating. The Ion Bernstein wave must be launched with electric field parallel to the magnetic field, rather than perpendicular to it as with fast-wave schemes. An attractive possibility is to use dielectric loaded waveguide as the launcher. This option is currently being studied.

The absorption efficiency of the waves at the resonance within the plasma is theoretically a very complicated matter. It involves calculating the launching, propagation, mode-conversion and absorption of the wave in the strongly inhomogeneous plasma medium. Although the physics of ICRF is not fully understood, which is an important reason for doing the experiments, solutions in one dimension of the wave equations can be obtained from numerical codes[12]. Studies carried out on the anticipated Alcator C-Mod plasmas show that for the D(He^3) option the theoretical absorption in a single pass through the plasma is about 10%, with perhaps a further 10% mode converted to Bernstein waves. Previous experience indicates that this absorption level is probably sufficient to ensure reasonable overall efficiency, since the waves reflect from the plasma edge and hence make multiple passes through the plasma. The hydrogen minority D(H) case has a much higher theoretical single-pass absorption, typically 50% or more. The IBW half-harmonic heating is a nonlinear process that is less well understood theoretically. However, if the nonlinear absorption is insufficient, the addition of a small He^3 minority should provide almost complete linear absorption only about 6cm from the plasma center. Thus all three ICRF candidates look like feasible schemes and it will be of great interest to

compare their effectiveness.

In addition to the main ICRF program, the option of heating by electron cyclotron resonance absorption (ECH) appears very attractive. The physics of absorption and the design of launching structures are in many respects more straightforward for ECH. Theoretical efficiencies are close to 100% and the control of the power deposition location is very good. The major difficulty is the absence of appropriate wave sources. The frequency required is in the vicinity of 140-250 GHz for magnetic fields of 5 to 9 T. Gyrotrons with megawatt-level power are just becoming available at around 140GHz, but extensive development will be needed to reach the higher frequencies we require. If ECH is pursued for CIT the sources will have to be developed. Then Alcator C-Mod would be an ideal testbed for their application. In addition to transmission and launching technology studies, the ability to do local heating and hence profile control would make experiments at even only a 1 MW level an important physics program.

11 Diagnostics

A major part of the experimental effort on any plasma experiment is devoted to the determination of the parameters of the plasma: diagnostics. To some extent, the diagnostic systems are separate from the machine itself and subject to modification and improvement. However, to give an impression of the capabilities anticipated for Alcator C-Mod, Table 3 gives a list of the diagnostic systems presently available or under development. The majority of these will be installed from the beginning of operation.

12 Research Program

The research program for Alcator C-Mod in its first few years is focussed on investigating the physics outlined in the four objectives stated earlier.

With first plasma operation, on the completion of construction, scheduled for mid 1990, the initial phases will be devoted to learning how to operate the tokamak. There are substantial unknown physics issues here. Bre-

akdown and plasma initiation requires appropriate control of the poloidal field null and evolution. In the presence of the thick vacuum vessel and superstructure the eddy currents make this a substantially more complex task than in previous tokamaks. Similarly, control of the plasma shape and position, especially during the ramp-up of the current, are much more elaborate issues with a strongly shaped machine. Further complications arise because of the large eddy currents in the structures. This early plasma operation will give the first opportunity to explore the ohmic performance and to investigate topics that relate to it such as fuelling, impurity behaviour, divertor operation, and confinement. Operation and debugging (with plasma) of the many diagnostics will also begin at this stage. It is anticipated that this initial phase will take about six months, assuming that no unforseen difficulties arise.

The second phase of operation, lasting about six months, includes the first stages of the ICRF heating operation. Exploring antenna loading and learning how to couple the power will undoubtedly require considerable time. Concurrently the ohmic and magnetic aspects of the plasma operation will be brought up to full performance and optimization studies conducted on confinement. The divertor studies will include the investigation of open versus closed and limiter versus divertor effects, as well as the optimization of divertor action for impurity control and fuelling.

The third phase of operation will see high power ICRF heating applied to plasmas that are well-controlled and able to run in optimum divertor configuration. Investigation of the confinement performance under such circumstances will involve the search for improved confinement regimes such as H-mode[9] (which is not necessarily achievable with ICRF alone in Alcator C-Mod) and P-mode[4] (enhanced confinement with density profile peaking). Exploration of the extremes of plasma shaping in this phase will contribute to our understanding of the value of advanced shaping for plasma performance. Toward the end of this phase, which may last perhaps two years, it is hoped that high frequency gyrotrons should be available and therefore the physics and technology of ECH can begin to be incorporated into the Alcator program. This provides a means for support of the development of ECH as an alternative scheme for CIT, but also more specifically enables the pursuit of temperature profile control to begin.

The future of an experimental program beyond five years becomes rather

harder to predict, since it depends to an increasing extent on the outcomes of the earlier stages and of experiments elsewhere. However, current-profile control seems a potentially very profitable line of research which we anticipate being part of the Alcator program. In addition to the anticipated ECH program, we have the sources (4MW at 4.6 GHz) built up during the Alcator C program, to study lower hybrid current drive. Non-inductive current drive is a topic of great long term importance in fusion. Moreover the flexibility, as well as high performance, designed into Alcator C-Mod will make it a very appropriate vehicle for the pursuit of tokamak research on topics that progress may reveal to be of future significance. It is anticipated that Alcator C-Mod will remain a valuable and profitable research resource for the plasma fusion program into the late 1990s and possibly beyond.

13 Predicted Performance.

To predict the plasma parameters that will be obtained on Alcator C-Mod requires assumptions to be made about confinement and heating, based on past experience in tokamak research. There is no ab initio theory which we can use with any confidence to predict the transport properties of tokamaks, but there are several fairly well established "scaling laws", based on fits to experimental data from many different machines, that form the basis of the present predictions and indeed the predictions concerning other planned machines such as CIT. These laws, particularly those which include auxiliary heating effects, are based primarily on experiments in much lower density plasmas; their validity is thus uncertain. Of course, one purpose of the Alcator C-Mod experiments is to see whether in fact the plasma obeys these laws and whether the predicted parameters are in fact achieved. Therefore the material of this section should be regarded as only our best estimate of what the plasmas will be like.

13.1 Density

The range of density over which a tokamak can operate is limited at the low end by runaway of the electrons and formation of energetic tails to the electron distribution and also sometimes by the dominance of impurity species over the working gas. The highest density that a tokamak can achieve is generally limited by the occurrence of MHD instabilities that give rise to

disruptions and catastrophic quenching of the plasma current. This maximum achievable density is often called the density limit.

The cause of the density limit appears to be radiative cooling of the edge of the plasma that gives rise to a contraction of the current profile and eventually MHD instability. The balance between radiative loss and ohmic heating explains to some extent the well established observation that the density limit depends on the plasma current-density. This dependence has traditionally been incorporated by expressing the density in terms of a "Murakami number" : $\bar{n}_e R/B_T$. This accounts for the fact[13] that the central current density in a circular tokamak is generally proportional to B_T/R. Typically the limit on the Murakami number is observed to be roughly 0.6×10^{20} m^2T^{-1}, although the exact value depends on a variety of factors. A slightly different approach championed by Greenwald[14] is to regard the important current density as being the mean over the plasma cross-section. The Greenwald limit is then $\bar{n}_e/\kappa\bar{j} \approx 10^{20}$ m^{-1} MA^{-1}. For a 3MA, 9T, $\kappa = 1.8$ plasma in Alcator C-Mod, these density limits are respectively about 8 and 20 $\times10^{20}$ m^{-3}. A valuable contribution from the experiments on Alcator C-Mod will be to help to distinguish between these two limits.

It is generally the upper end of the density range that is of most interest. However the flexibility of the machine is enhanced by a wide density range. Alcator C was able to operate at densities down to a few times 10^{19} m^{-3}. We anticipate that Alcator C-Mod will have similar capability.

13.2 Energy Confinement

Perhaps the aspect of plasma performance most difficult to predict is the energy confinement time. The electron transport in tokamaks is always anomalously large compared to that predicted on the basis of purely collisional (neoclassical) diffusion. There is mounting evidence that the ion transport is also very often anomalous. The fits to empirical data from a variety of experiments that we use for the prediction of Alcator C-Mod performance are that the energy confinement time, τ_E, is given by one of the following scalings:

1. NeoAlcator Confinement[3]

$$\tau_E^{NA} = 2\times10^{-21}\ \bar{n}_e\ a\ R^2\ \kappa^{1/2} \qquad s.$$

2. Kaye-Goldston (L-Mode)[15]

$$\tau_E^{KG} = 0.055(I_p/MA)^{1.24}\ B^{-0.09}(\bar{n}_e/10^{20})^{0.26}\ R^{1.65}\ a^{-0.49} \times \kappa^{0.28}(P_t/MW)^{-0.58}\ \ s.$$

3. Neoclassical Ion Transport

$$\tau_{Ei}^{NC} = 10^7\ I_p^{\ 2}\ (T_i/keV)^{1/2}\ (R/a)^{1/2}\ n_e^{\ -1}\ K_2^{\ -1} \qquad s.$$

Units here are S.I. except where specified otherwise and P_t indicates the total heating power in the plasma. The collisionality coefficient, K_2, is that given by Chang and Hinton[16]. Its value is 0.66 for low collisionality and inverse aspect ratio.

The NeoAlcator confinement time describes the scaling for ohmically heated tokamaks in moderate density regimes, while the Kaye-Goldston scaling is appropriate for auxilliary-heated tokamaks. Both of these are the total confinement time including both electron and ion transport. However, the losses have normally been considered to be dominantly in the electron channel. Therefore, for the purposes of our estimates, we take the power loss via the electrons to be $3n_eT_e/2\tau_{Ee}$, where the electron confinement time is given by

$$1/\tau_{Ee} = 2\sqrt{[(1/\tau_E^{NA})^2 + (A_{KG}/\tau_E^{KG})^2]}.$$

This form adds the two empirical loss terms in quadrature, thus making a conservative estimate of confinement; the factor of two makes the loss via the electrons contribute the total energy loss (when the electron and ion energy contents are equal). An anomaly factor, A_{KG}, in the Kaye Goldston component is included to allow variable amounts of confinement deterioration.

The Neoclassical ion confinement time is an approximation to the losses anticipated from the theoretical neoclassical ion thermal conduction. (The power loss is $3n_iT_i/2\tau_{Ei}$). Experimental observations of saturation of ohmic confinement at high density can be reasonably modelled using purely NeoAlcator electron losses (A_{KG}=0) by taking the ion losses to be an anomally factor, A_{NC}, times the neoclassical value. Typically, to model Alcator C results[4], gas fuelled plasmas required ion losses such that $A_{NC}\approx 3$ but pellet-fuelled plasmas required no anomally ($A_{NC}\approx 1$). The experiments also indicate that the anomalous loss in the gas-fuelled case is indeed in the ion channel. An alternate scaling, taking A_{NC}=1 but using the Kaye-Goldston scaling (A_{KG}=1), also reproduces the global confinement time for gas fuelled cases reasonably well; although it attributes saturation to additional electron losses, in

contradiction to the experimental indications.

A slightly different scaling also has received considerable attention recently, namely the original Goldston scaling[17]:

$$\tau_E^G = 0.037\ (I_p/MA)\ R^{1.75}\ a^{-0.37}\ \kappa^{0.5} \quad s.$$

This fits experiments (on various machines) with auxilliary heating. However, for Alcator C it gives confinement times that are typically a factor of two lower than what was observed for gas fuelled cases and than the Kaye-Goldston scaling. This factor of two discrepancy with Kaye-Goldston is present also for the high densities typical of Alcator C-Mod but in view of the Alcator C experience we regard Goldston confinement as probably unduly pessimistic for C-Mod.

Calculations of the energy confinement time and the accompanying ion and electron temperatures have been performed with a zero-dimensional model, in which the electron and ion energy balance equations, coupled by the collisional exchange of energy, are solved self-consistently with the total heating and loss terms for the two species. Profile factors are accounted for using parabolas to variable power. The density for the results that will be shown is taken to be $\propto(1-r^2/a^2)^{0.5}$, where r is the midplane minor radius of the assumed concentric elliptical flux surfaces. The temperature profile exponent is taken to be that value which is consistent with a current density profile proportional to $T_e^{3/2}$ and safety factor of 1 on axis. The ion temperature profile is effectively the same relative shape as the electron temperature profile. More elaborate one-dimensional calculations have also been done. Their results agree with the corresponding zero-dimensional cases, within the uncertainties of the confinement scaling model. Therefore we give only the zero-dimensional results here.

In Fig. 14 we show the total confinement time predicted for a full-performance ohmic Alcator C-Mod plasma, as a function of central density. (Parameters assumed for this and the following cases are: R=.665m, a=.21m, κ=1.8, B_T=9T, I_p=3MA, Z_{eff}=1). The three cases shown are for: 'P' mode, NeoAlcator electrons and 1× Neoclassical ions (A_{KG}=0, A_{NC}=1); 'G' (gas) mode, NeoAlcator electrons and 3× Neoclassical ions (A_{KG}=0, A_{NC}=3); and 'K-G', Kaye-Goldston electrons and 1× Neoclassical ions (A_{KG}=1, A_{NC}=1). It may be observed that the G and K-G modes give very similar confinement while the P-mode enhancement is noticeable at high density. Fig. 15 gives the electron and ion temperatures for two cases using G-mode confinement assumptions. The ohmic

case is exactly that for the previous figure. For essentially the whole density range the electrons and ions are closely coupled, having temperatures between about 3.5 and 2 keV: very significant performance for an ohmic plasma. The second case shown assumes that an additional heating power of 4MW is deposited in the ions (modelling in an oversimplified way the anticipation that the bulk of the ICRF power will go into ion heating). At high densities the species are again well coupled, with temperature around 4.5 keV. However, at the lower end of the density range the ions become decoupled from the electrons and a hot ion mode appears, with temperatures to 20 keV and beyond.

As can be seen in Fig. 16, this hot ion mode is accompanied by an increase of the total confinement time relative to ohmic. This is because more of the plasma energy is in the ions, which have good confinement, than in the electrons for the ion heated case. A K-G calculation shows essentially the same effect but has lower confinement at high density. If the ion transport anomaly is a strong function of ion temperature (or temperature profile, as for η_i mode losses) naturally these predictions might be altered. The Alcator C-Mod experiments provide a good opportunity to investigate such issues, which are critical for future experiments.

As a summary of the anticipated performance we can plot these results in Fig. 17 as Lawson parameter, $n_e\tau_E$, versus T_i. The plot includes lines of D-T equivalent Q, the power factor that would be achieved for a pure 50-50 mix of deuterium and tritium; Q=1 corresponds to "breakeven" and Q = ∞ to "ignition". Also, we show a variety of historically achieved values from various tokamaks. The Alcator C-Mod predictions consist of the density scans, plotted as lines on the figure; the uppermost end of the lines are at $n_{e0}=10^{21}$ m^{-3}. Ohmic P and G mode scalings are shown, while the 4MW ion heating case shown is for K-G scaling, which is the most conservative (P mode comes almost to the Q=1 line at the highest density). A striking aspect of these results is that the predicted performance in Alcator C-Mod exceeds the present achievements of the flagship tokamaks TFTR and JET, which are 3 to 4 times bigger and at least ten times more expensive.

While these remarkable parameters await the operation of Alcator C-Mod for their verification, this comparison does illustrate graphically the potential benefits of high-field high-density tokamaks for pursuing the plasmas needed for fusion.

14 Conclusions

Alcator C-Mod incorporates various innovative engineering concepts, which will provide valuable experience in the development of engineering techniques for high-field compact fusion experiments. Its predicted plasma performance is outstanding for a tokamak of such modest size and cost, and it therefore represents a very effective vehicle for the study of plasma confinement close to ignition conditions. The program we have outlined is focussed toward resolving issues that are crucial for the achievement of fusion ignition in the near future, but it also addresses many questions of fundamental long term importance to our understanding of the physics of magnetic confinement. The flexibility of Alcator C-Mod ensures that it can be used to pursue appropriate research objectives and hence will be productive in fusion research for a long time to come.

Acknowledgements

Many colleagues and technical staff at the Plasma Fusion Center and elsewhere have contributed to the development of the designs and plans described here. We are grateful to them all.

The Alcator experiments are supported by the U.S. Department of Energy under contract DOE-AC02-78ET51013.

References

1. M.Greenwald et al Phys.Rev.Lett., 53, 352 (1984).
2. R.J.Hawryluk et al, in *Plasma Physics and Controlled Nuclear Fusion Research*, (Proc. 11th Int. Conf., Kyoto) I.A.E.A. Vienna (1986), vol 1, p 51.
3. R.R.Parker, M.Greenwald, S.C.Luckhardt, E.S.Marmar, M.Porkolab and S.M.Wolfe, Nucl.Fusion, 25, 1127 (1985).
4. M.Greenwald et al, in *Plasma Physics and Controlled Nuclear Fusion Research*, (Proc. 11th Int. Conf., Kyoto) I.A.E.A. Vienna (1986), vol 1, p 139. Also S.M.Wolfe, M.Greenwald, R.Gandy, R.Granetz, C.Gomez, D.Gwinn, B.Lipschultz, S.McCool, E.Marmar, J.Parker, R.Parker, J.Rice, Nucl.Fusion, 26, 329 (1986).
5. M.Porkolab, J.J.Schuss, B.Lloyd, Y.Takase, S.Texter, et al, Phys.Rev.Lett., 53, 450 (1984)
6. J.Freidberg, M.Greenwald, D.Gwinn, I.Hutchinson, B.Lipschultz, E.Marmar, D.B.Montgomery, R.R.Parker, M.Porkolab, J.Schultz, D.Sigmar, R.Thome, S.M.Wolfe and T.Yang, *Alcator C-Mod Proposal,* MIT Plasma Fusion Center report PFC/RR-85-18(1985).
7. P.Bonoli, M.Greenwald, D.Gwinn, I.Hutchinson, B.Lipschultz, E.Marmar, D.B.Montgomery, R.R.Parker, R.Pillsbury, M.Porkolab, J.Ramos, D.Sigmar, R.Thome, S.M.Wolfe, *Alcator C-Mod Proposal Addendum*, MIT Plasma Fusion Center(1986).
8. e.g. I.H.Hutchinson J.Fusion Energy, 6, 257 (1987).
9. F.Wagner et al, Phys.Rev.Lett., 49, 1408 (1982).
10. S.C.Jardin, N.Pomphrey and J.DeLucia, J.Comp.Phys., 66, 481 (1986).
11. D.A.Humphreys and I.H.Hutchinson, Bull.Am.Phys.Soc., 32, 1924 (1987).
12. M.Brambilla submitted to Nucl.Fusion.
13. M.Murakami, J.D.Callen and L.A.Berry, Nucl.Fusion, 16, 347 (1976).
14. M.Greenwald, J.Terry, S.Wolfe, S.Ejima, M.Bell, S.Kaye and G.H.Neilsen, MIT Plasma Fusion Center report PFC/JA-86-22 (1986) submitted to Nucl.Fusion.
15. S.M.Kaye and R.J.Goldston, Nucl.Fusion, 25, 65 (1985).
16. C.S.Chang and F.L.Hinton, Phys.Fluids, 25, 1493 (1982).
17. R.J.Goldston, Plasma Phys. and Controlled Fusion, 26, 87 (1984).

Figure Captions

Fig.1 Cutaway drawing of Alcator C-Mod.

Fig.2 Elevation of Alcator C-Mod.

Fig.3 Concept for the toroidal field coil sliding joint assembly.

Fig.4 Detail of the sliding joint design, showing the finger shaping and feltmetal pads.

Fig.5 Perspective CAD drawing of the OH solenoid, showing the two parts OH1 and OH2.

Fig.6 The vacuum vessel. Thickwall stainless steel construction is used.

Fig.7 Standard equilibrium flux surfaces, showing the plasma diverted into the bottom divertor.

Fig.8 The profiles, for the equilibrium of Fig.7, of (a) Toroidal current density, (b) Safety factor, as a function of poloidal flux, normalised to the 95% value.

Fig.9 Sequence of plasma shapes for a current ramp up and flat-top calculated with TSC. The time covered by this sequence is the first 2 seconds of plasma.

Fig.10 Evolution of toroidal field (a), plasma current (b), and plasma density (c) in the TSC simulation of Fig.9.

Fig.11 The axisymmetric model for eddy-current calculations. Blocks show the finite coil elements of the active and passive structures. The flux contours are calculated for a startup scenario in which a good field null for breakdown is obtained, including effects of all the eddy currents.

Fig.12 The ion cyclotron resonant frequencies relevant to Alcator C-Mod ICRF,

hydrogen (f_{cH}), deuterium (f_{cD}), and helium-3 (f_{cHe3}) frequencies are shown. The source frequency at 80 MHz is resonant at different operating magnetic fields.

Fig.13 The ICRF antenna shown mounted in the port of Alcator C-Mod.

Fig.14 Predicted energy confinement time versus central density for ohmically heated plasmas.

Fig.15 Electron and ion central temperatures predicted for ohmic and ion-heated plasmas using the "G" (gas-fuelled) confinement assumptions. (NeoAlcator electron and 3× Neoclassical ion losses).

Fig.16 Comparison of the confinement predicted for ion-heated and ohmic cases for G-mode. Also shown (dashed) is the result for K-G (Kaye-Goldston electron) confinement assumptions in the heated case.

Fig.17 Ignition plot of Lawson parameter ($n_e \tau_E$) versus central ion temperature. Predicted lines for density scans in Alcator C-Mod are compared with historically achieved values. The ion-heated case uses Kaye-Goldston scaling.

Table 3: ALCATOR C–MOD DIAGNOSTIC SYSTEMS

Diagnostic Technique	Parameters	Features
Nd:YAG Thomson Scattering	$T_e(r,\theta, t)$; $n_e(r,\theta,t)$	50 Hz rep. rate, 2-d profiles
Dual Wavelength Interferometer	$n_e(r,t)$	Multi-Chord, CW operation. Able easily to follow density rise with pellet injection.
Electron Cyclotron Emission		
a) Fast Scanning Michelson	$T_e(r,t)$	Complete Spectra
b) Multi-Channel Grating Spectrometer	$T_e(r,t)$	Complete time histories at discrete radial points.
Neutral Particle Energy Analysis	$T_i(r,t)$; Ion Distribution Function	Two systems: one perpendicular, one tangential
Neutron Diagnostics		
a) ^{3}He Spectrometer	$T_i(r=0,t)$	
b) BF_3 Long Counter Array	Total Neutron Flux	
c) NE-213 Spectrometer	Energy Spectra of both D-D and D-T produced neutrons	
Visible and UV Spectroscopy		
a) 2.2 Meter Grazing Incidence Time Resolving Spectrograph	Line Emission	Covers any 40 Å slice between 18 Å and 600 Å with 4 msec time and 0.2 Å spectral resolution
b) 0.125 Meter Far UV Monochromator	Line Emission	1200 Å$< \lambda <$ 2300 Å
c) 0.2 Meter Extreme UV Monochromator	Line Emission	400 Å$< \lambda <$ 1500 Å
d) 1.0 Meter Normal Incidence Time Resolving Spectrograph	Line Emission Doppler broadening, shifts	1200 Å$< \lambda <$ 8000 Å
e) Visible continuum	$n_e^2 \times Z_{eff}/\sqrt{(T_e)}$	One 16 channel tangential array, plus a single chord system.
g) Periscope	Tangential View in Visible Light	2 systems

X-ray Diagnostics		
a) Compact Curved Crystal Time Resolving Spectrograph Arrays	$T_i(r,t)$; $T_e(r,t)$; $n_o(r,t)$	1.5 keV < $h\nu$ <5 keV, Measures Doppler broadening of impurity lines.
b) Broad Band Soft X-Ray Arrays	Plasma position and shape; MHD activity; impurity transport	Fully two-dimensional tomographic reconstructions.
c) HgI_2 Pulse Height System	$T_e(r,t)$; Electron tails	5 keV < $h\nu$ < 100 keV, 500 eV resolution
d) Flat crystal monochromator	Line and Continuum Emission	1 keV < $h\nu$ < 8 keV, 50 eV resolution
e) NaI Array	Hard X-rays produced at walls and limiter/ divertor plate structures as well as from non-thermal plasma electrons	0.5 MeV < $h\nu$ < 20 MeV, spatially resolved
f) Pinhole Camera	Tangential Image of Soft X-Ray Emission	
Bolometry	Total radiated plus charge exchange power from plasma	Spatially Resolved
CO_2 Scattering	Fluctuations; Driven lower hybrid, ICRF waves	
Langmuir Probes	Edge temperature and density profiles	Poloidal and radial scanning capability with multi-probe arrays.
Infrared Surface Temperature Measurements	Limiter/divertor plate surface temperatures	2-d imaging
Reflectometer	Edge Density Profiles	
Lithium Pellet Injector	Current Density Profile	
Laser Blow-Off Impurity Injector	Impurity Transport, Confinement	
Time of Flight Low Energy Neutral Spectroscopy	Edge T_i and neutral density	10 eV < E < 2000 eV

Fig 1

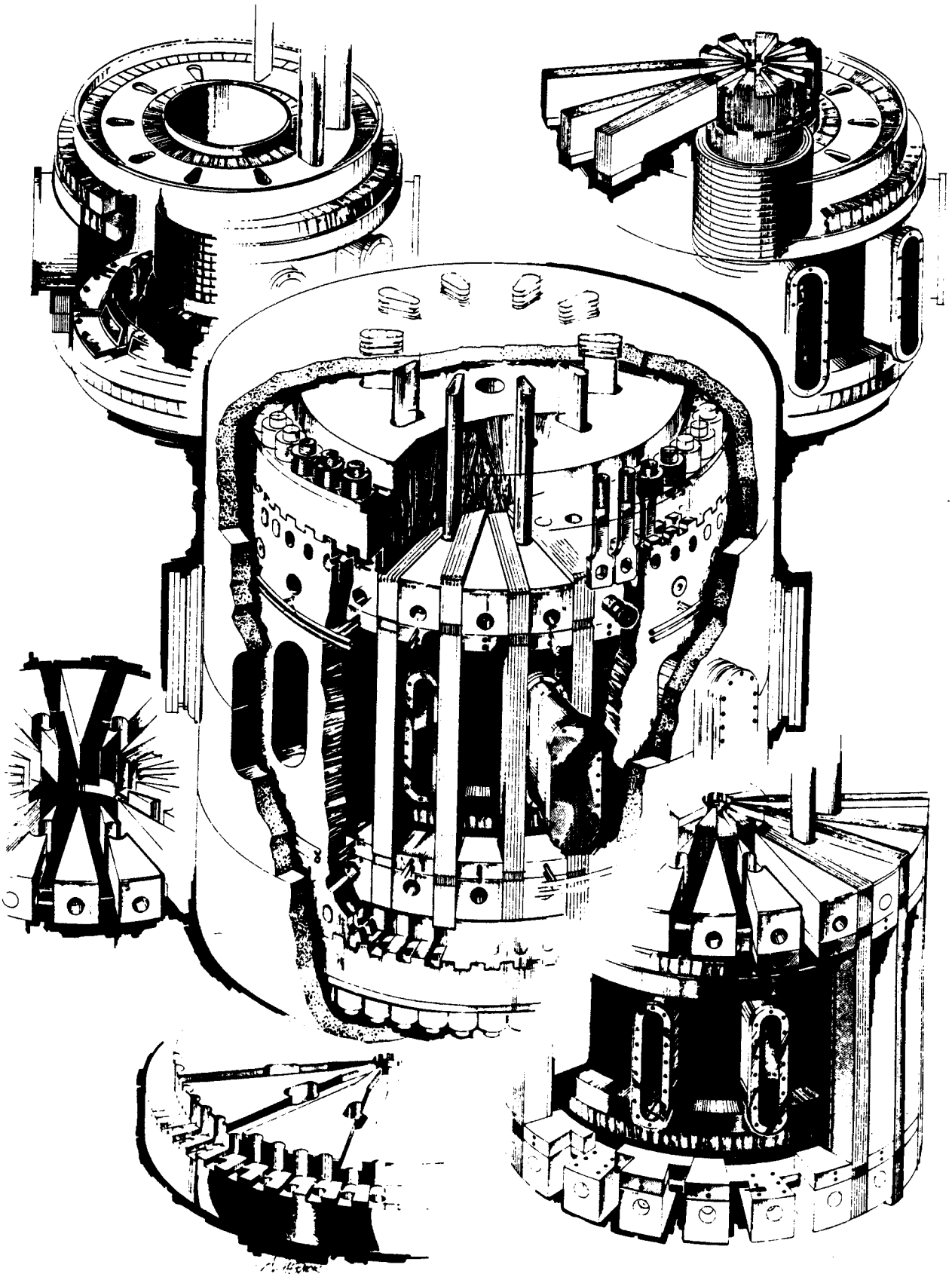

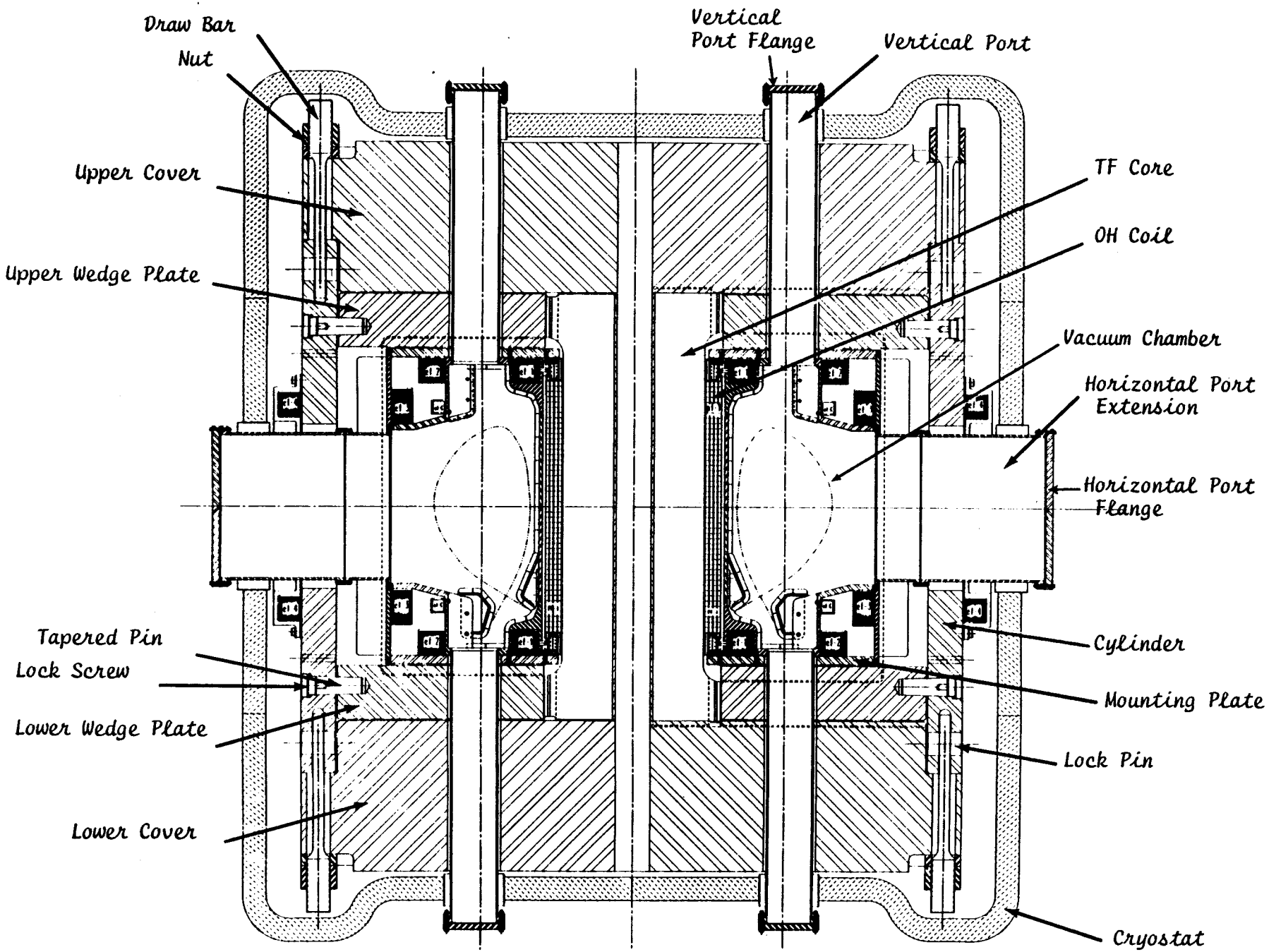
Draw Bar
Nut
Vertical
Port Flange
Vertical Port
Upper Cover
TF Core
OH Coil
Upper Wedge Plate
Vacuum Chamber
Horizontal Port
Extension
Horizontal Port
Flange
Tapered Pin
Lock Screw
Cylinder
Mounting Plate
Lower Wedge Plate
Lock Pin
Lower Cover
Cryostat
ALCATOR C-MOD

Fig 7

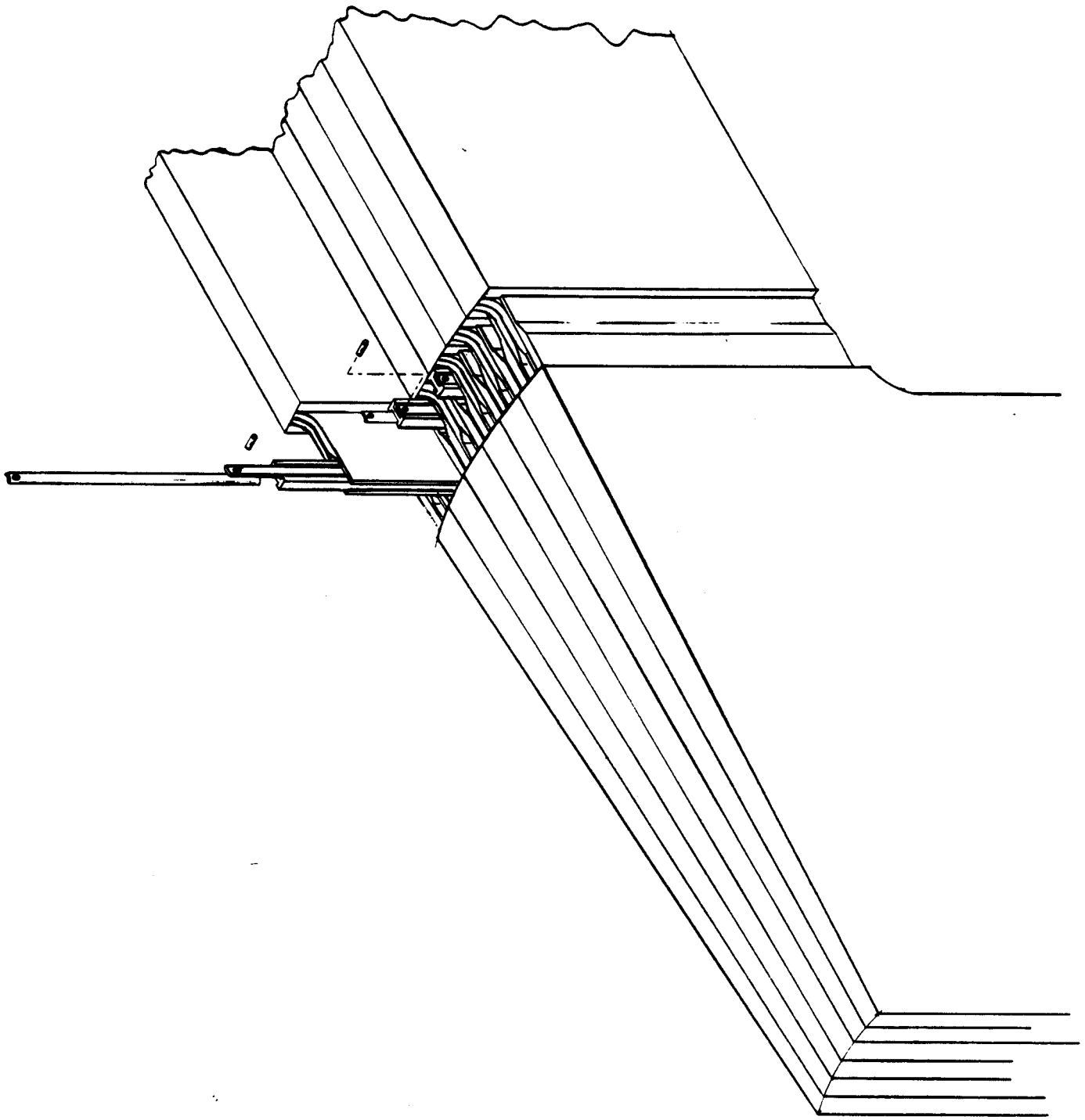

Fig 3

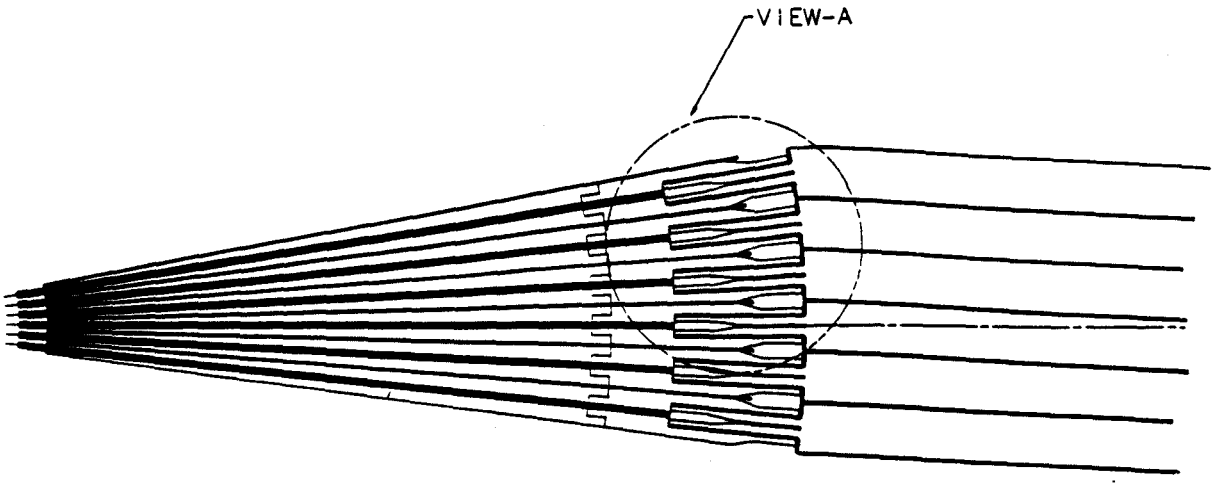

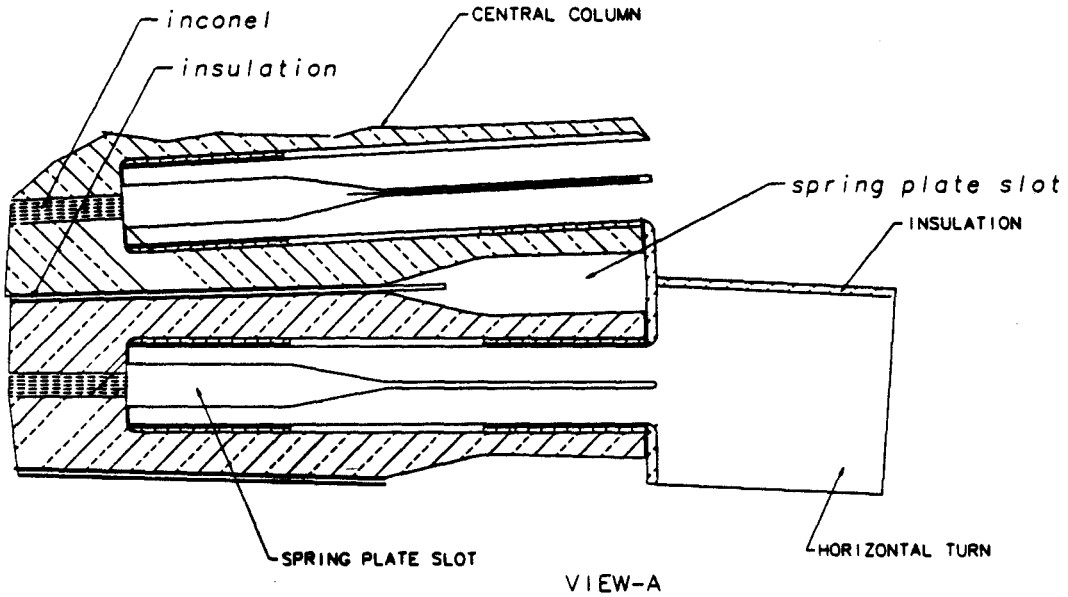

VIEW-A
SCALE-4:1

Fig 4

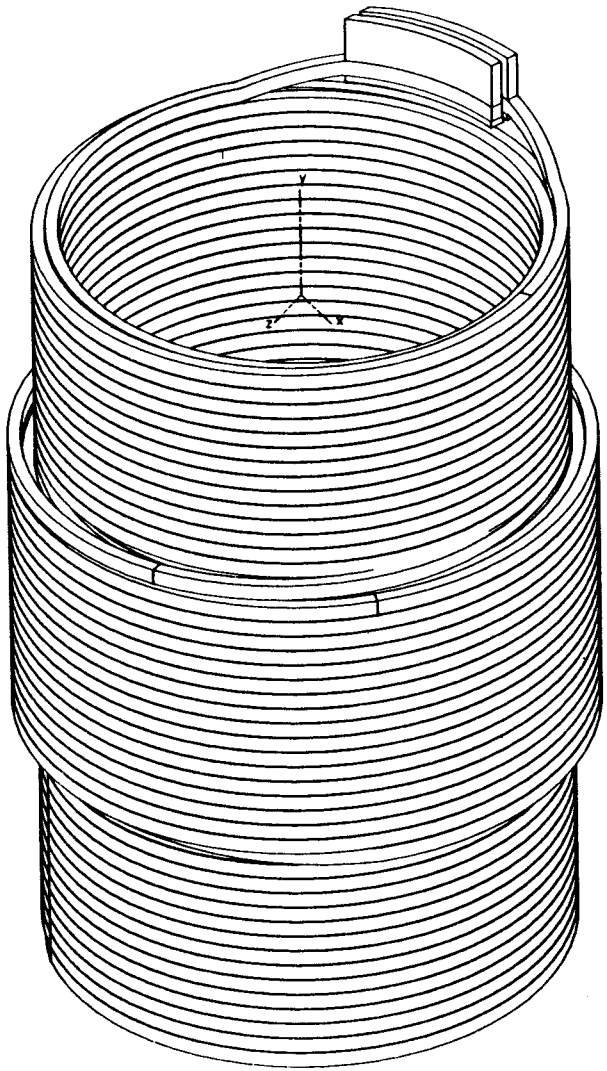

OH1

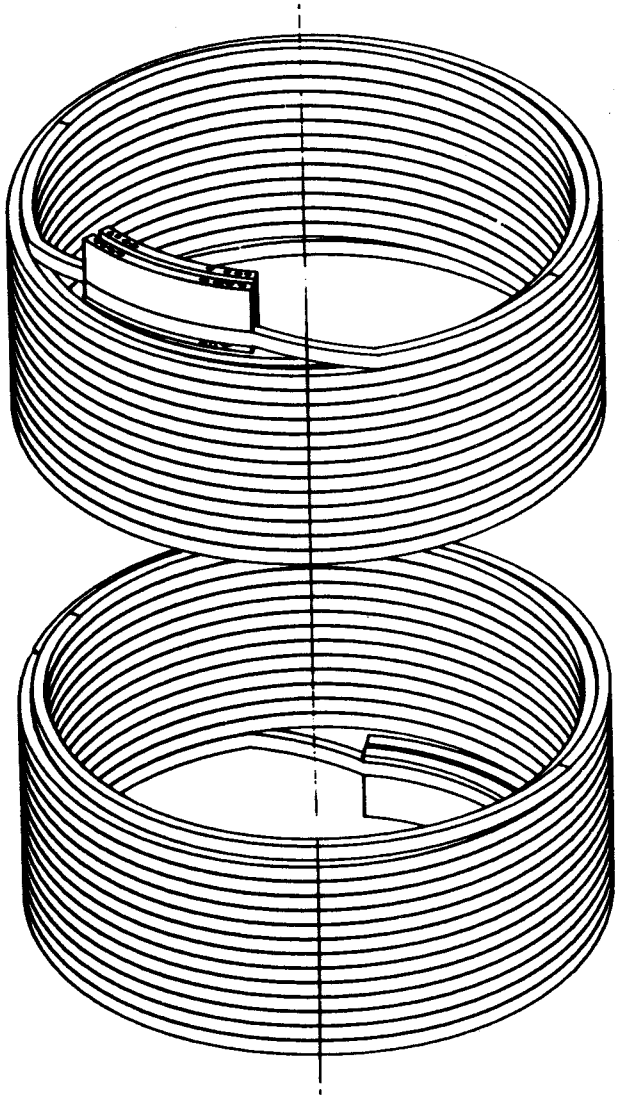

OH2

Fig 5

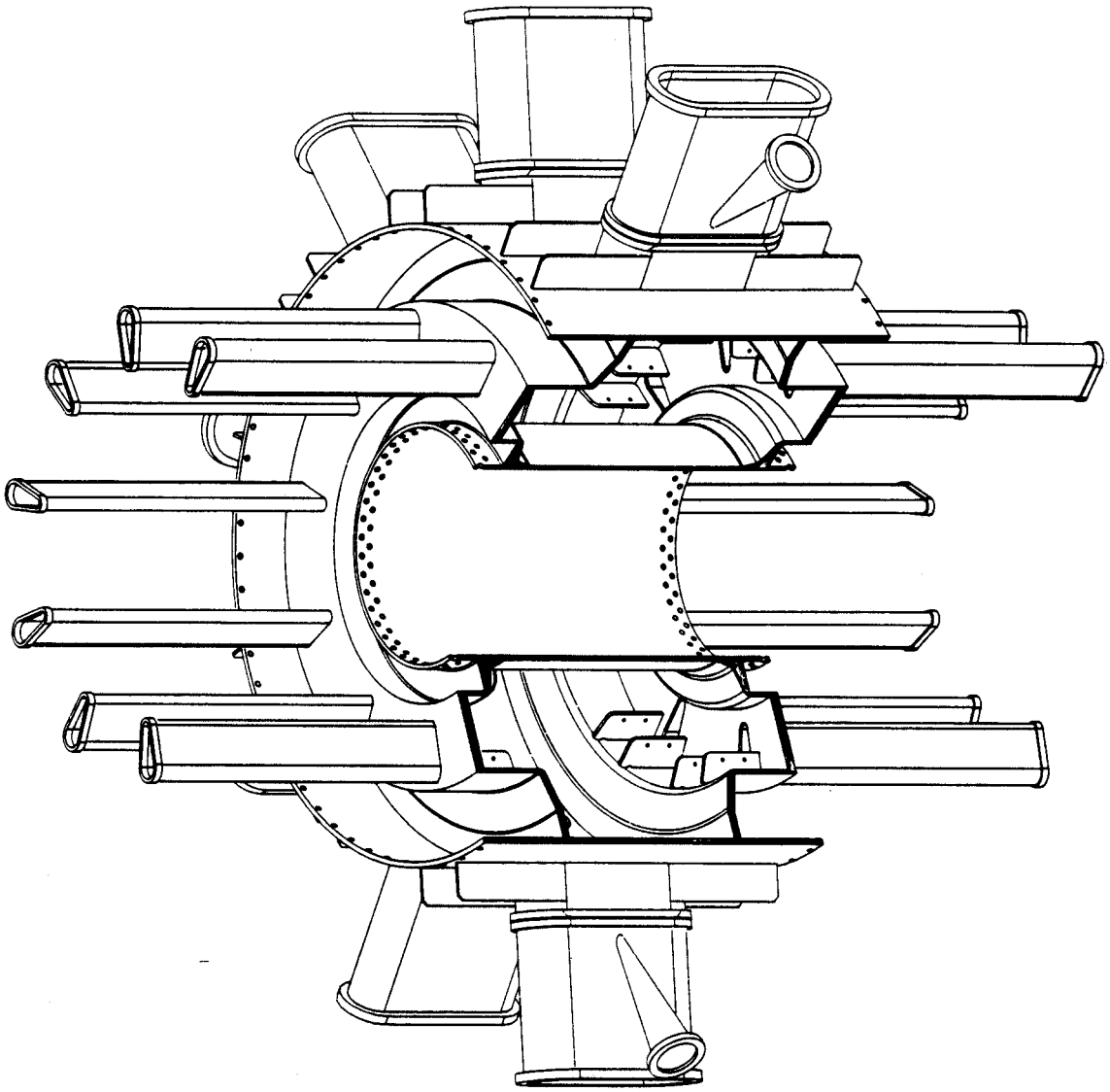

Fig 6

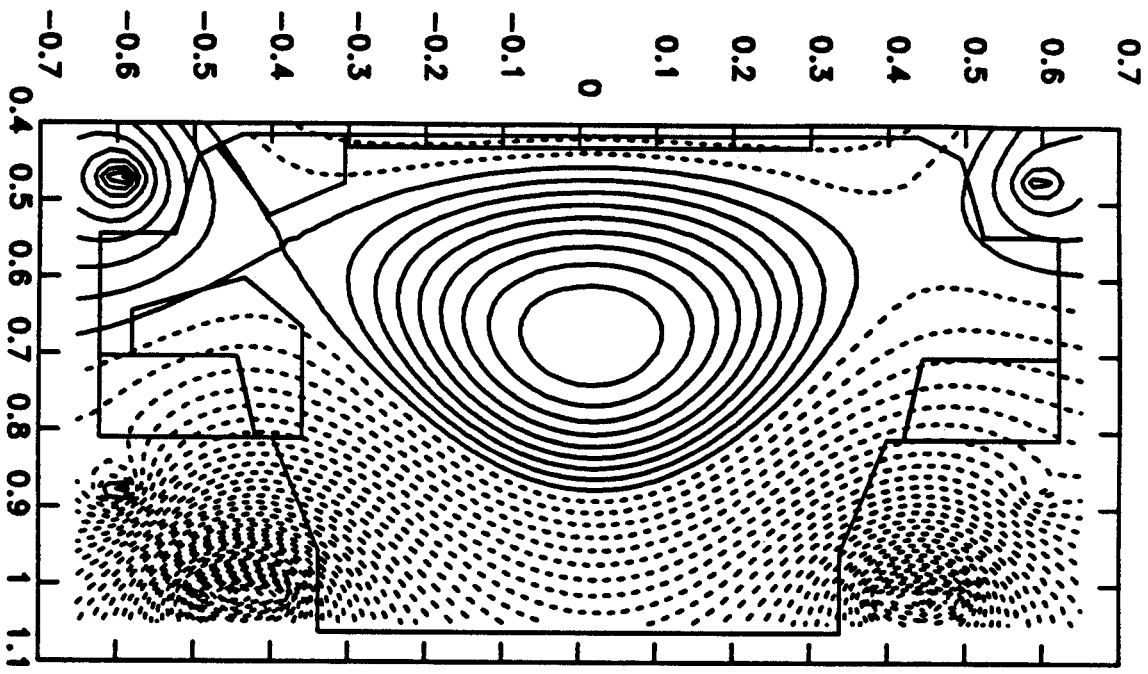

Fig 7

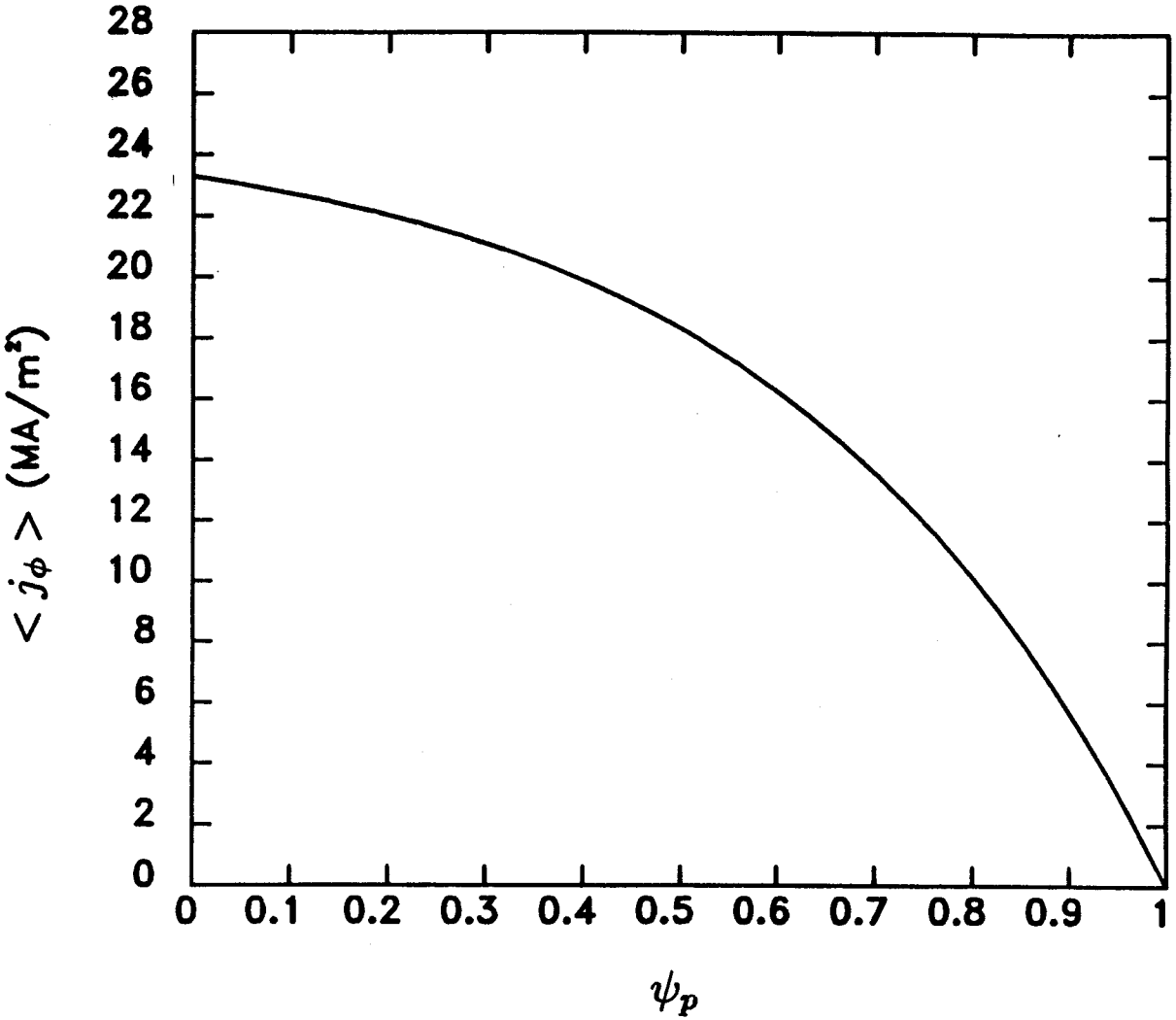
28
26
24
22
20
18
16
14
12
10
8
6
4
2
0
$< j_\phi >$ (MA/m^2)
0
0.1
0.2
0.3
0.4
0.5
0.6
0.7
0.8
0.9
1
ψ_p

Fig 8(a)

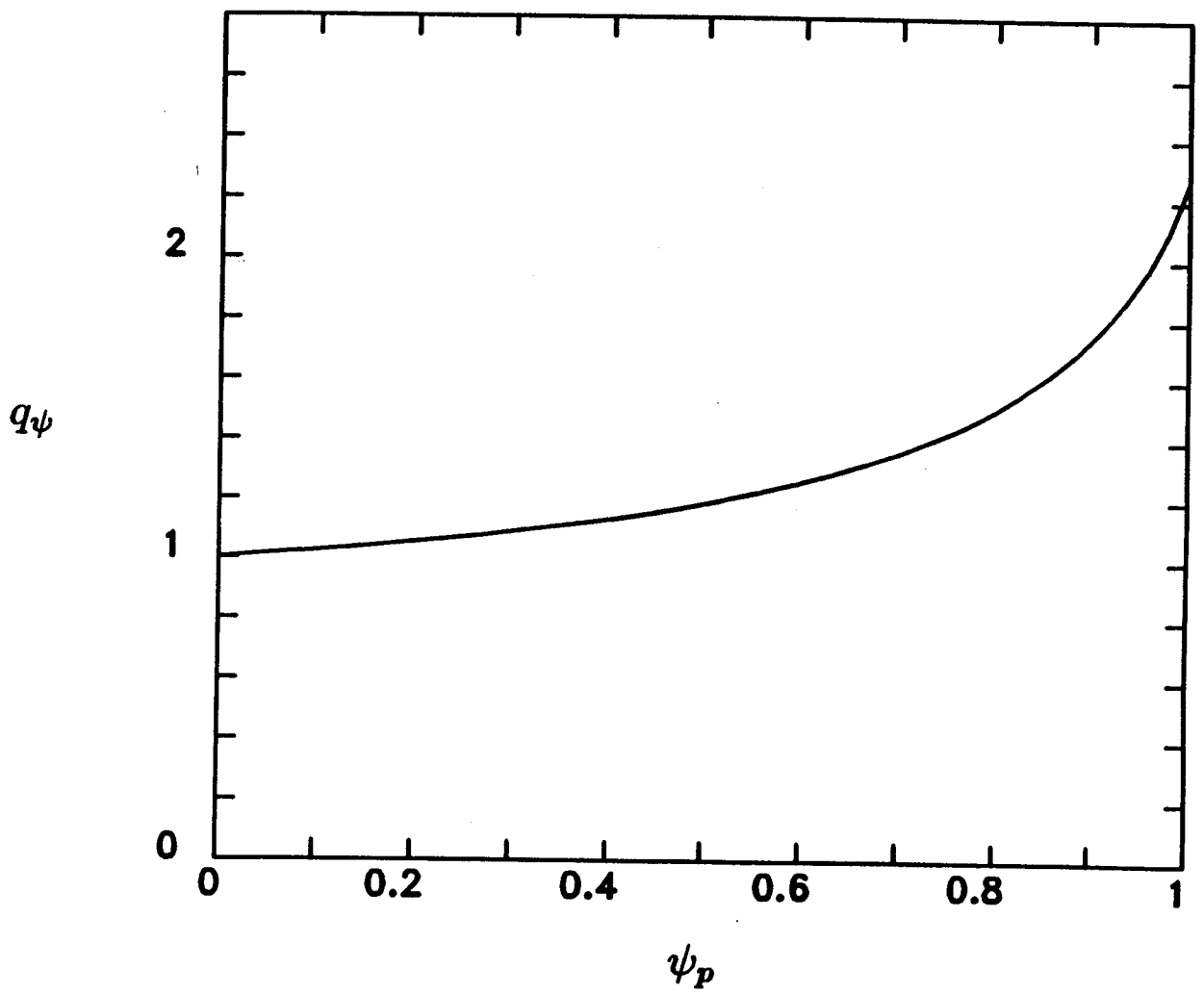

Fig 8(b)

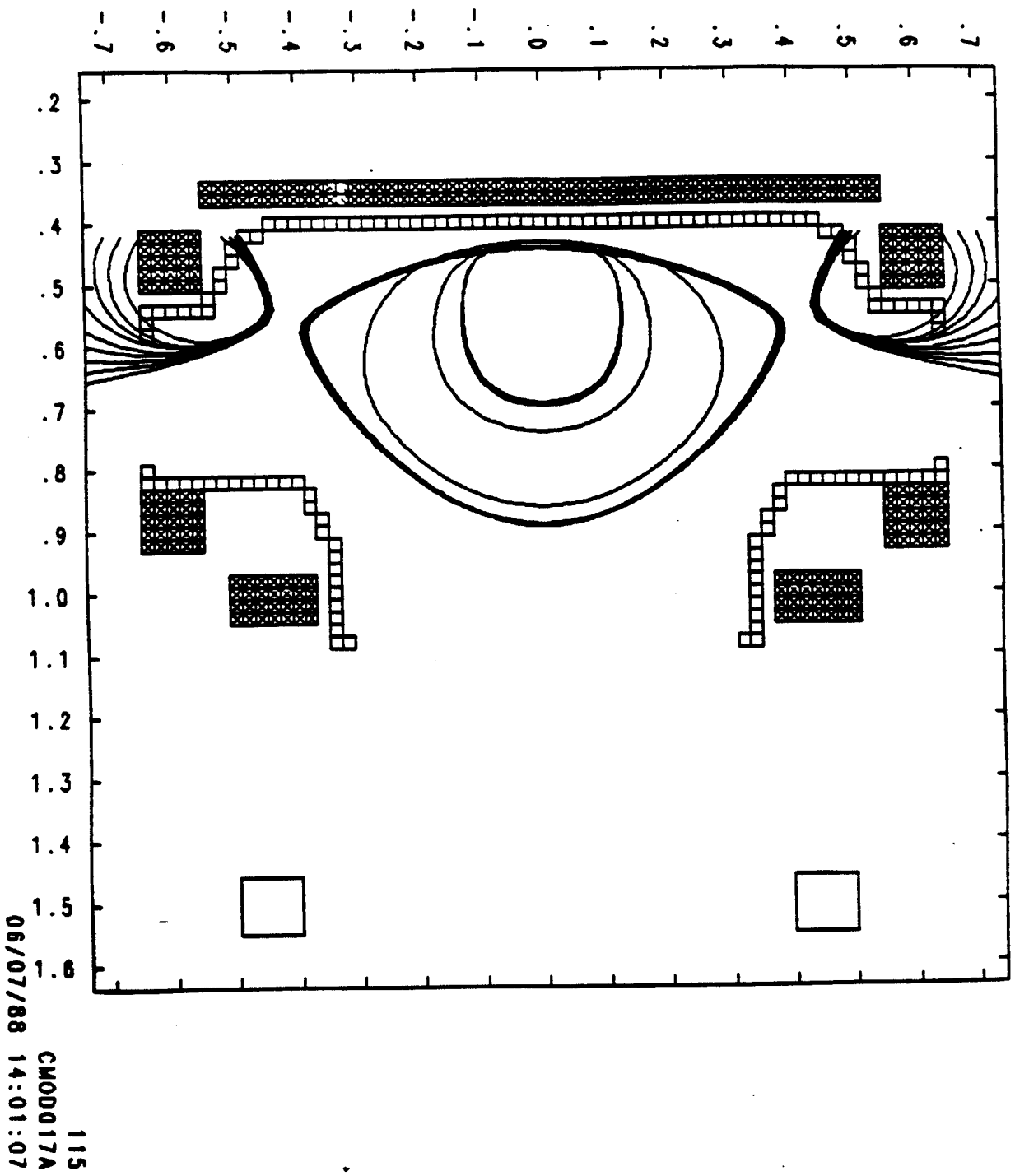
-.7 -.6 -.5 -.4 -.3 -.2 -.1 .0 .1 .2 .3 .4 .5 .6 .7
.2 .3 .4 .5 .6 .7 .8 .9 1.0 1.1 1.2 1.3 1.4 1.5 1.6
06/07/88 14:01:07
CMOD017A
115

Fig 9

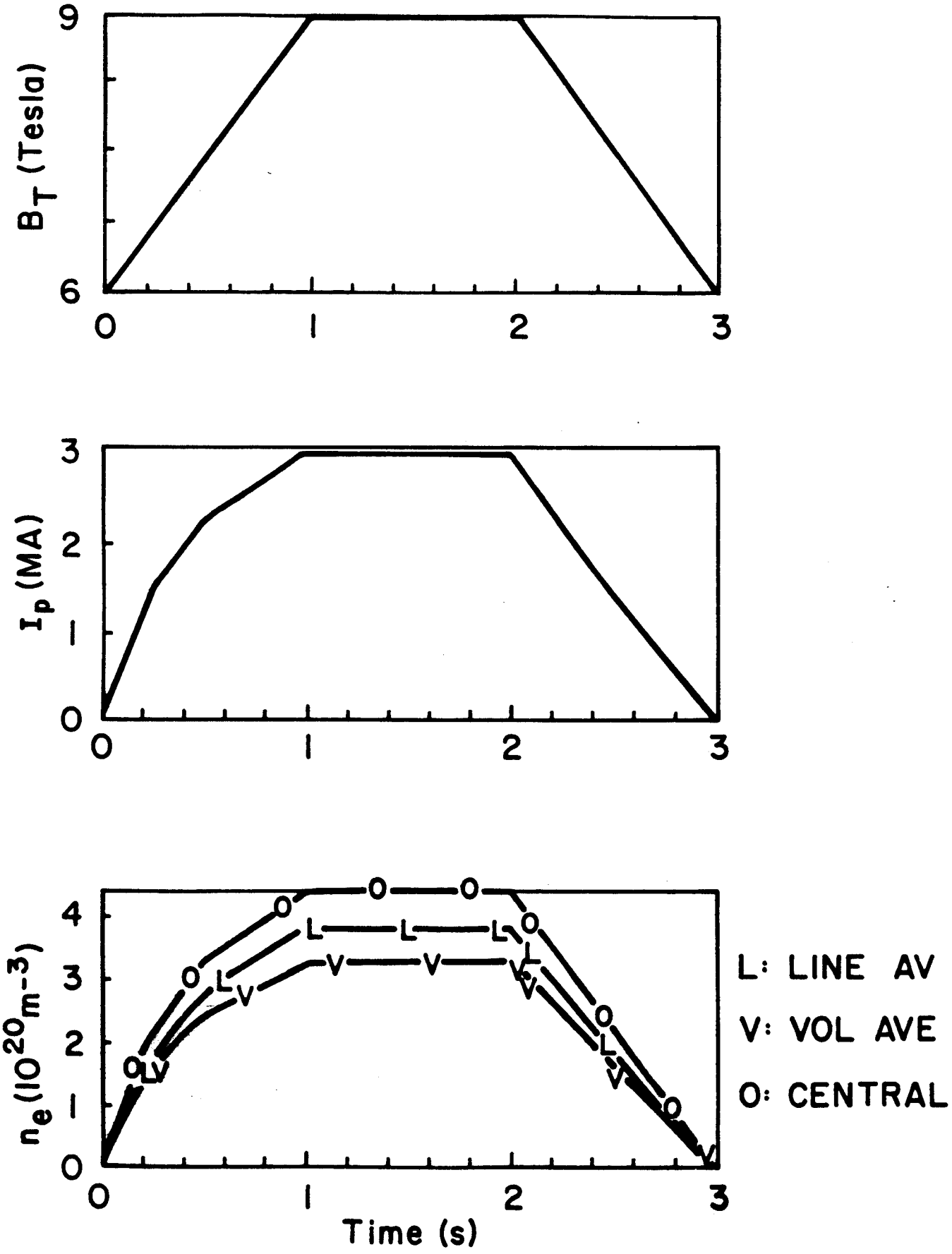
B_T (Tesla)
9
6
0
1
2
3
I_p (MA)
3
2
1
0
$n_e(10^{20}m^{-3})$
4
3
2
1
Time (s)
L: LINE AV
V: VOL AVE
O: CENTRAL

Fig. 10

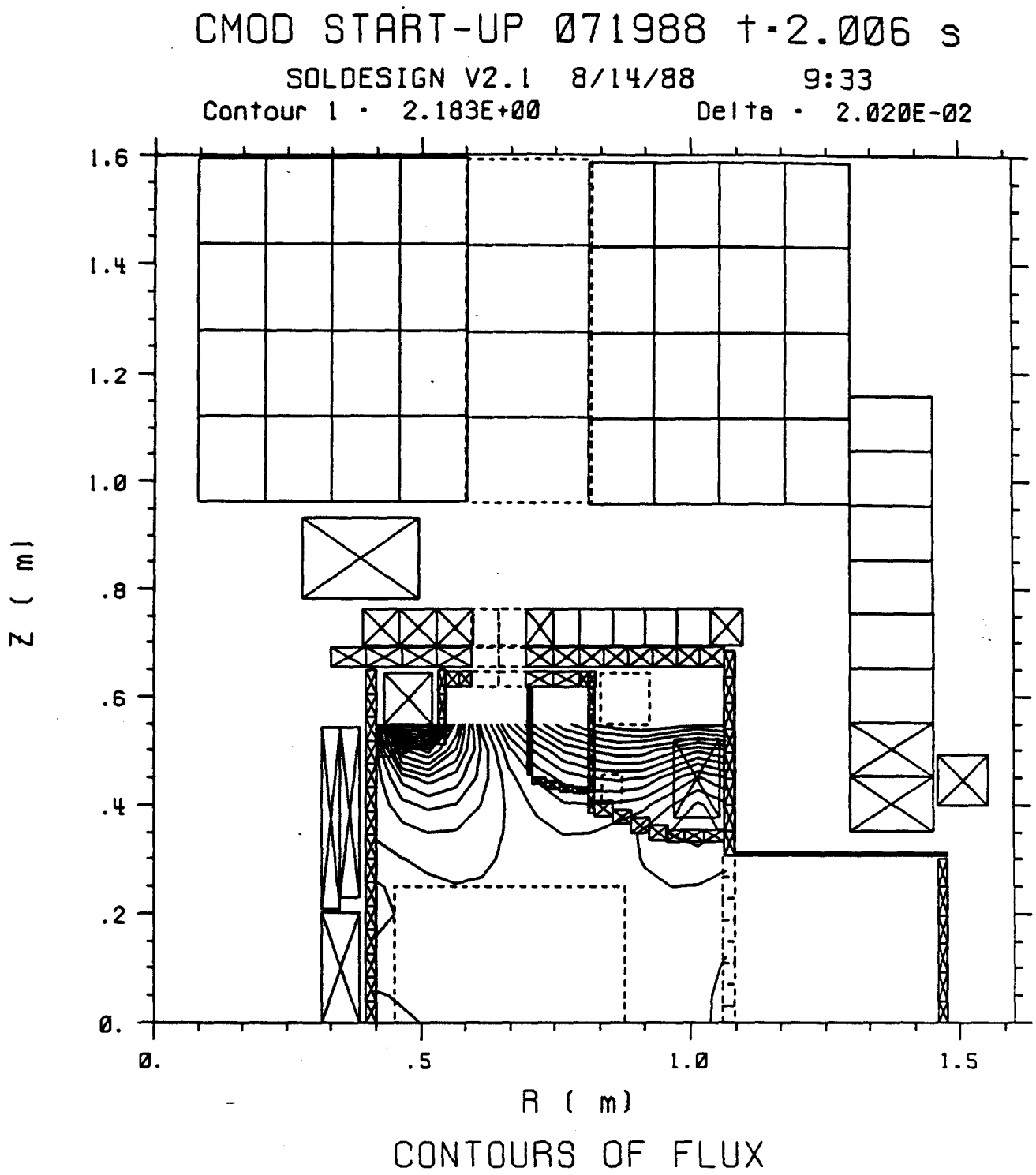
CMOD START-UP 071988 t-2.006 s
SOLDESIGN V2.1 8/14/88 9:33
Contour 1 - 2.183E+00 Delta - 2.020E-02
1.6
1.4
1.2
1.0
.8
.6
.4
.2
0.
Z (m)
0.
.5
1.0
1.5
R (m)
CONTOURS OF FLUX

Fig 11

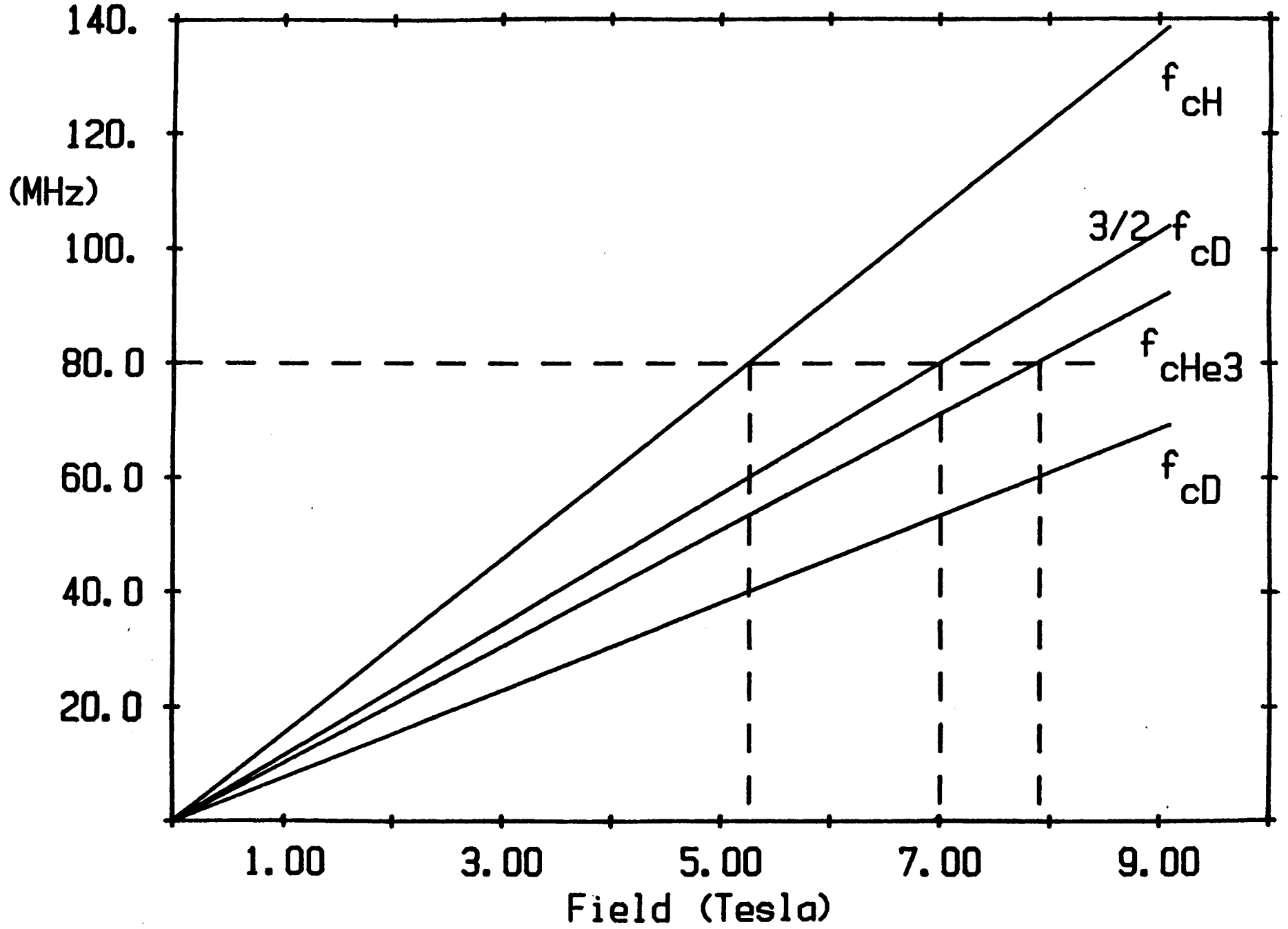
140.
120.
(MHz)
100.
80.0
60.0
40.0
20.0
1.00
3.00
5.00
7.00
9.00
Field (Tesla)
f_{cH}
3/2 f_{cD}
f_{cHe3}
f_{cD}

Fig 12

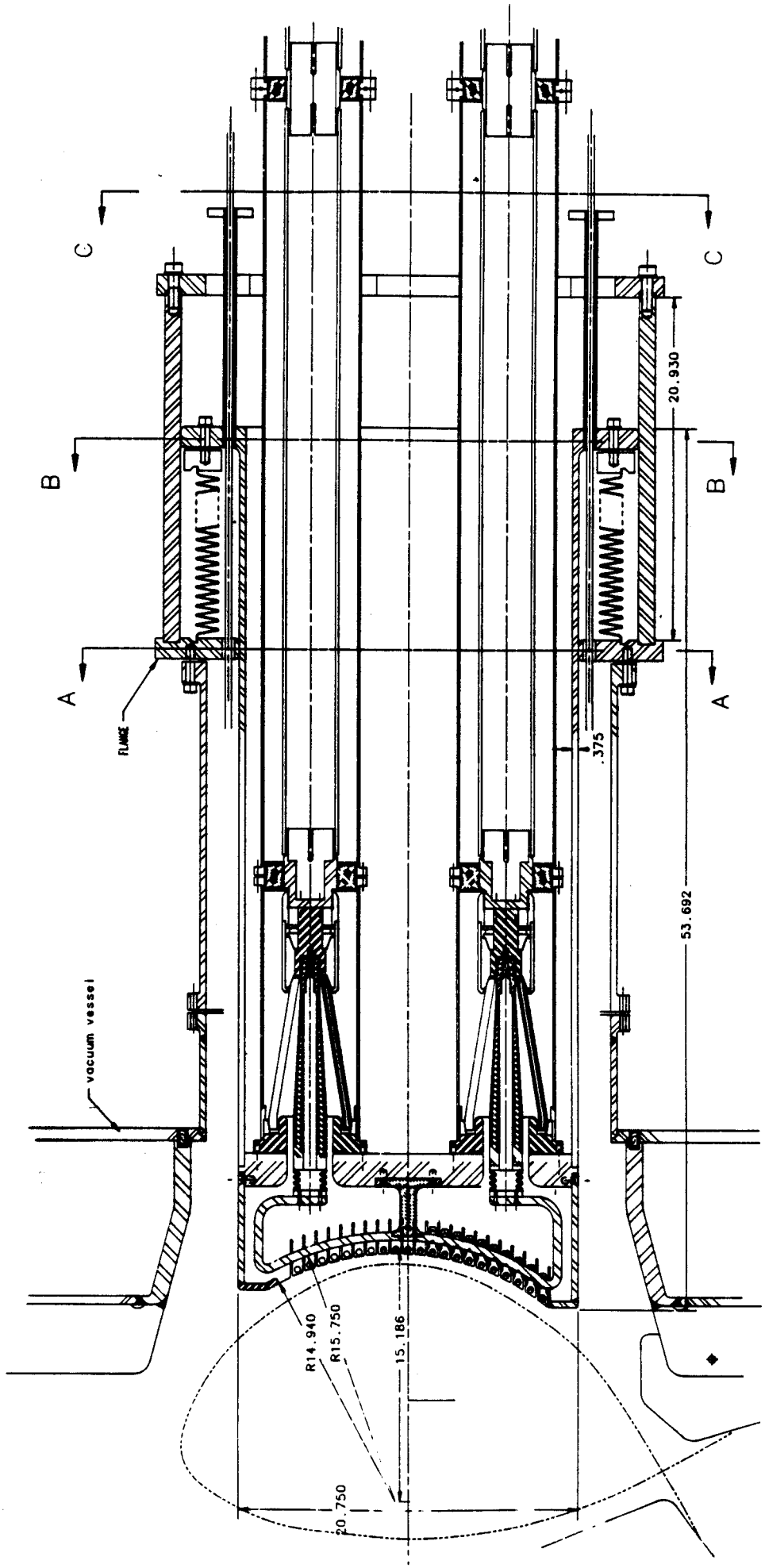
C
C
B
B
A
A
FLANGE
20.930
.375
53.692
vacuum vessel
R14.940
R15.750
15.186
20.750

Fig 13

τ_E (ms)
20.0
60.0
100.
140.
180.
n_{eo} ($/10^{20}$ m^{-3})
1.00
3.00
5.00
7.00
9.00
'P': $A_{NC}=1$
'G': $A_{NC}=3$
K-G

Fig 14

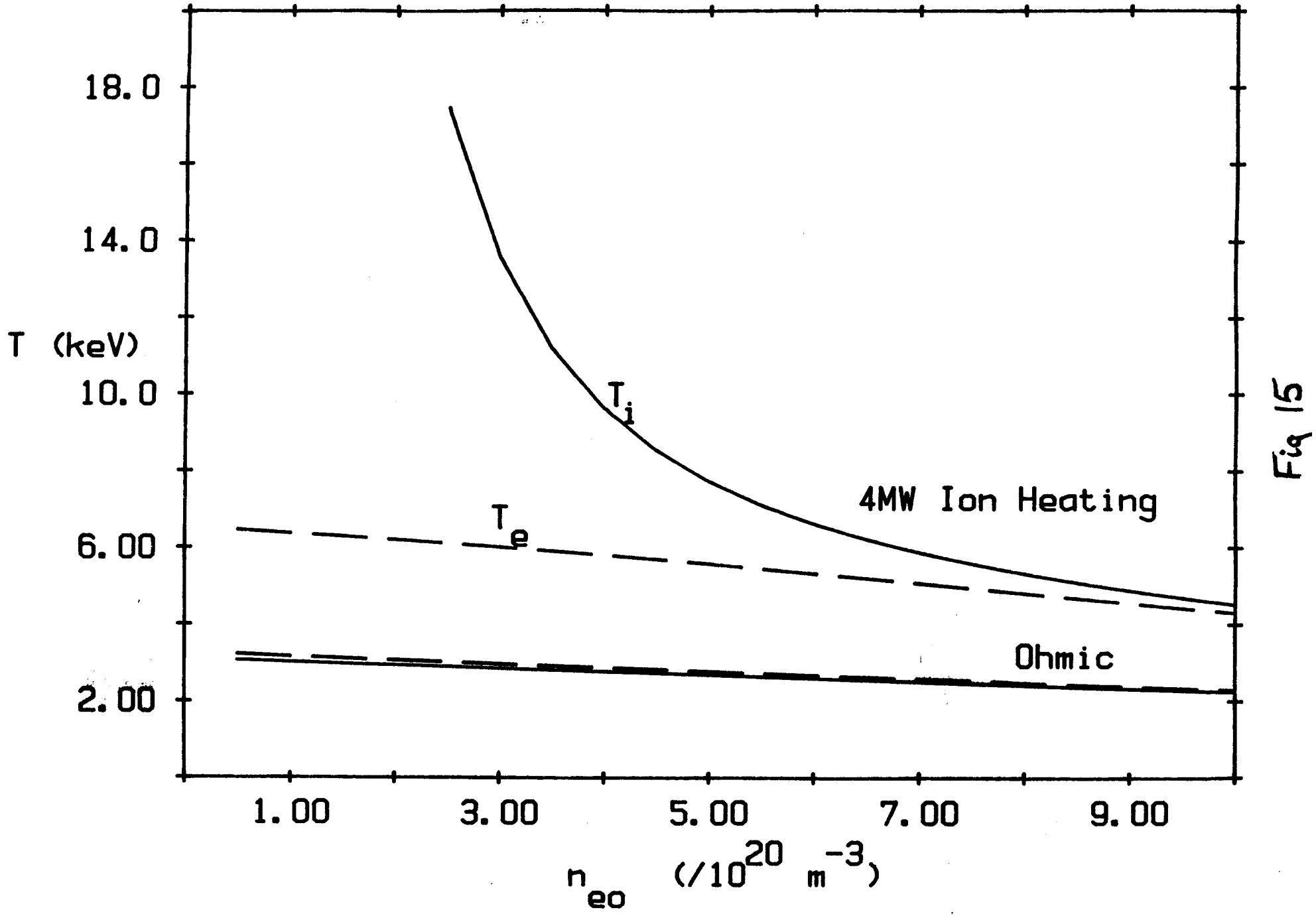
18.0
14.0
T (keV)
10.0
6.00
2.00
T_i
T_e
4MW Ion Heating
Ohmic
1.00
3.00
5.00
7.00
9.00
n_{eo} ($/10^{20}$ m^{-3})

Fig 15

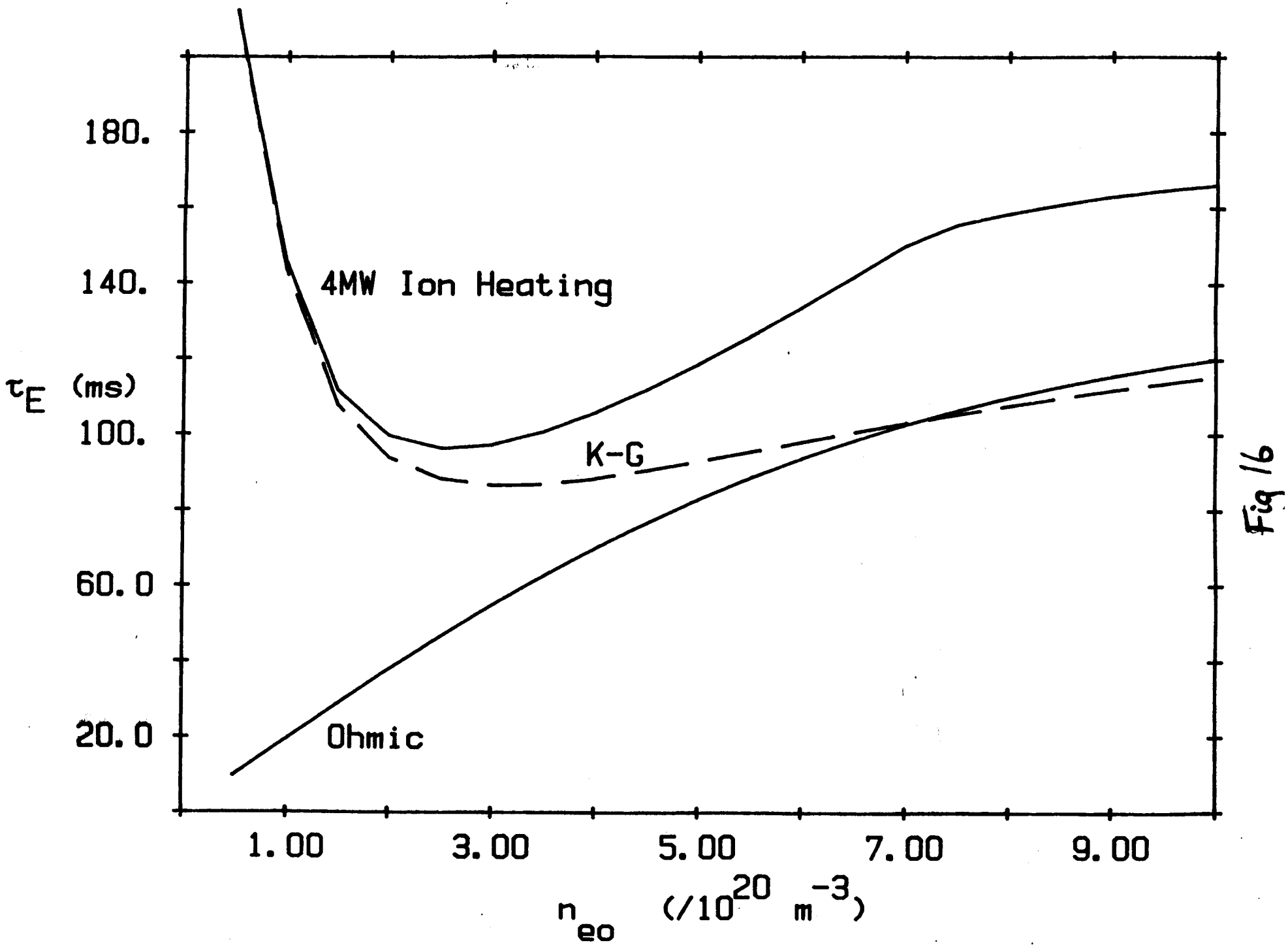
180.
140.
100.
60.0
20.0
τ_E (ms)
4MW Ion Heating
K-G
Ohmic
1.00
3.00
5.00
7.00
9.00
n_{eo} ($/10^{20}$ m^{-3})

Fig 16

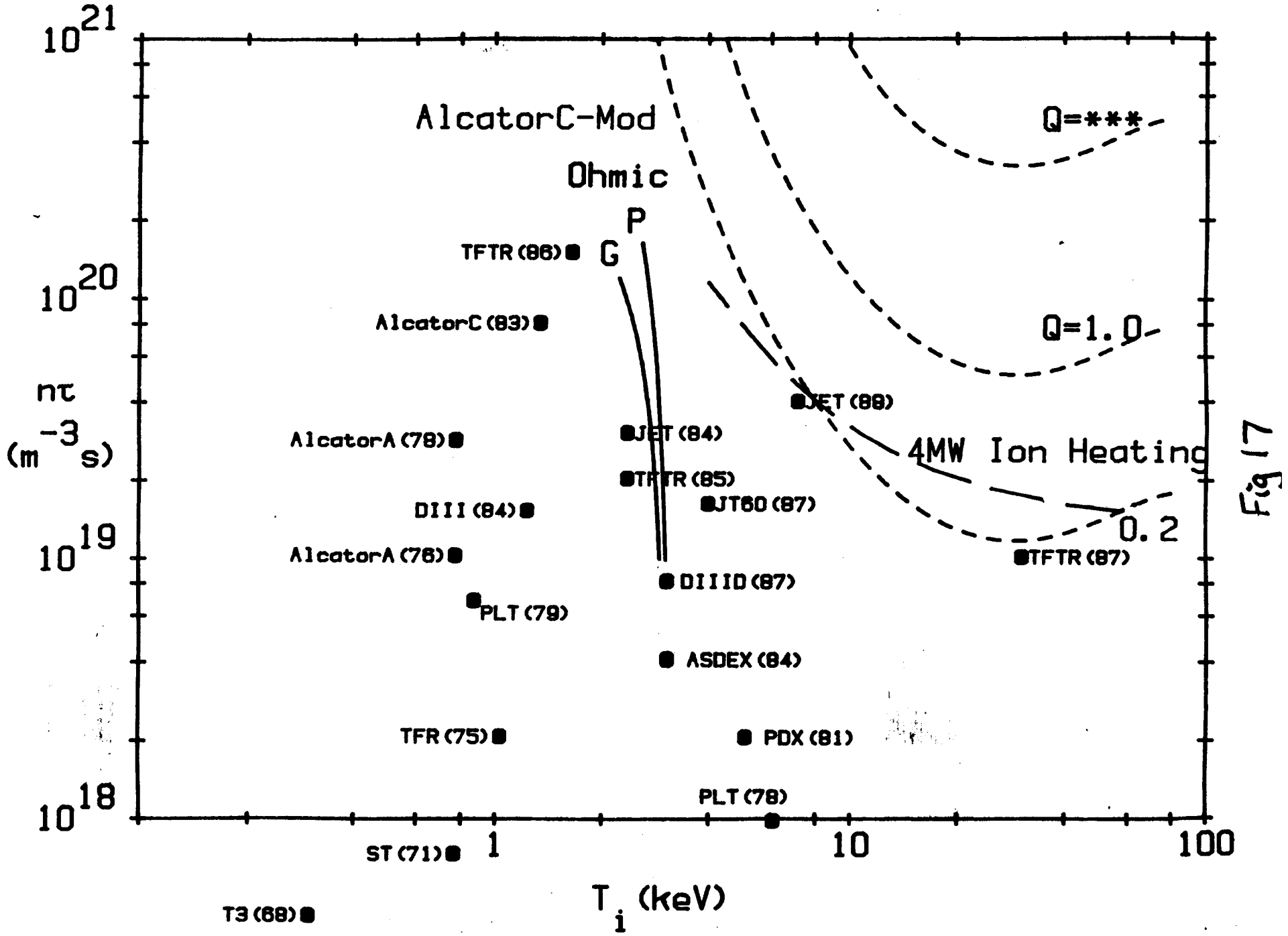
AlcatorC-Mod
Ohmic
P
G
Q=***
Q=1.0
4MW Ion Heating
0.2
TFTR (86)
AlcatorC (83)
AlcatorA (78)
DIII (84)
AlcatorA (76)
PLT (79)
TFR (75)
ST (71)
T3 (68)
JET (84)
TFTR (85)
JT60 (87)
DIIID (87)
ASDEX (84)
PDX (81)
PLT (78)
JET (88)
TFTR (87)
10^{21}
10^{20}
10^{19}
10^{18}
$n\tau$
$(m^{-3}s)$
1
10
100
T_i (keV)

Fig 17